MASTER'S DEGREE PROGRAMME

Eco-Energy Engineering

Development of a Molten Salt Parabolic Trough Test Platform Simulator for Training Purposes of the Operating Staff

SUBMITTED AS A MASTER THESIS

to obtain the academic degree of

Master of Science in Engineering (MSc)

by

Florian Bamberger

September 2018

Thesis supervisor

FH-Prof. DI Rudolf Kraft

PREFACE/ACKNOWLEDGEMENTS

This Master thesis is the result of a seven months ongoing engagement at German Aerospace Center (DLR) / Institute of Solar Research in Stuttgart. Studying Eco-Energy Engineering and getting the chance to work at a world-wide known research institution was my motivation to do this Master thesis.

I would like to thank my supervisors Daniel Högemann and Kareem Noureldin for their intellectual support and feedback during my engagement and for their time to do so. I also thank Dr. Tobias Hirsch for agreeing on the engagement and giving me the chance to participate to the 21. Kölner Sonnenkolloquium. Furthermore, I would like to thank everyone of the Solar Research team for the welcoming environment and the hobby-footballers for the time to blow the cobwebs away and for a lot of fun.

Many thanks also to my thesis supervisor of the University of Applied Sciences Upper Austria, FH-Prof. DI Rudolf Kraft, who has always been available if there have been any questions. His course about solar thermal power plants also contracted my passion for CSP technologies.

Although it is one´s own way, there are so many people paving parts of the way in social, occupational and other important areas. Many thanks to my friends and deep gratitude to my parents for their incessant support, not only financially but also mentally, during all the years.

SWORN DECLARATION

I hereby declare that I prepared this work independently and without help from third parties, that I did not use sources other than the ones referenced and that I have indicated passages taken from those sources.

This thesis was not previously submitted in identical or similar form to any other examination board, nor was it published.

.....

Florian Bamberger

Wels, September 2018

KURZFASSUNG

Kraftwerksbetreiber sind verantwortlich für die Kraftwerksintegrität, die Sicherheit der Mitarbeiter und die optimale Leistungsausbeute hochkomplexer Anlagen. Automatische Betriebsmodi unterstützen die Betreiber in der Regel bei der optimalen Betriebsführung von Großanlagen. Testanlagen zielen hingegen darauf ab, neue Technologien oder Komponenten zu etablieren und sind daher in den meisten Fällen kleiner in ihrer Ausführung und weniger automatisiert. Umso wichtiger sind erfahrene Betriebsleute die einen sicheren Betrieb der Testanlage garantieren können. Dasselbe gilt für Parabolrinnen-Testanlagen mit Flüssigsalz als Wärmeträgermedium. Es gibt kaum Erfahrungen im Betrieb mit Flüssigsalz im Solarfeld und die Komponenten und Regelstrategien können sich bei Testanlagen regelmäßig ändern. Unter Umgebungsbedingungen würde das Salz einfrieren, exzessive Temperaturgradienten könnten Komponenten beschädigen und das Flüssigsalz könnte sich bei Überhitzung zersetzen. Diese Herausforderungen im Betrieb mit Flüssigsalz erfordern vorab Trainings der Betriebsmannschaft, ohne dabei das Risiko von Materialbeschädigungen oder eine Gefährdung von Mitarbeitern oder der Umwelt einzugehen. Deshalb hat das Deutsche Zentrum für Luft- und Raumfahrt (DLR) im Zuge des "HPS2 – High Performance Solar 2" Projektes einen Simulator entwickelt, welcher den virtuellen Betrieb des Salzkreislaufes, und damit ein Einarbeiten vorab der Inbetriebnahme, erlaubt. Die Bedienoberfläche basiert auf Vorentwürfen des Bediensystems, welches von Siemens (SPPA-T3000) realisiert wird. Der Simulator ist grundsätzlich in LabVIEW programmiert, bedient sich jedoch einem Tool zur detaillierten Simulation transienter Vorgänge im Solarfeld. Das Tool, namens Virtual Solar Field, wurde vom DLR entwickelt und ist über eine TCP/IP Schnittstelle in den Simulator eingebunden. Das Anlagenmodell in LabVIEW enthält detaillierte physikalische Modelle des hydraulischen Netzwerks und des Speichersystems. Außerdem verfügt es über Steuerungen und Regelungen, sowie Schutzfunktionen und automatische Betriebsmodi, wie sie für die Leittechnik der realen Anlage definiert sind. Simulationen haben das korrekte Verhalten der physikalischen Modelle bestätigt. Gemessene Wetterdaten mit unterschiedlichen Wetterbedingungen zu verschiedenen Jahreszeiten stehen als vordefinierte Datensätze für Simulationen und Trainings zur Verfügung. Um Erfahrungen in der Betriebsführung eines solchen Parabolrinnen-Kreislaufes zu sammeln, kann das Anlagenmodell manuell bedient werden.

ABSTRACT

Power plant operators are responsible for plant integrity, staff safety and optimal performance of highly sophisticated facilities. Most commonly, large-scale power plants are highly automated. Test facilities, however, aim to provide evidence for the usability of new technologies or components. Consequently, test plants are mostly much smaller in capacity and to a lesser extend automated. The more important are skilled operators, who can safely run the test facility. The same applies to test facilities of parabolic trough power plants with molten salt as heat transfer fluid. The technologies and components used are novel, components or control systems can change regularly and there is no experience and no standards available for operation of parabolic trough solar fields with molten salt as working fluid. Under ambient conditions the salt would freeze, excessive temperature gradients could damage plant components and molten salt would decompose if overheated. Consequently, there exists the need to provide foregoing training to the staff with little risk of damage to the components and without endangering staff or the environment. Therefore, DLR developed a simulator for the test facility in the "HPS2 – High Performance Solar 2" project, which enables the virtual control of the salt cycle and allows to become acquainted with the behaviour of the test facility before commissioning. The human machine interface is based on pre-designs of the planned control system which will be done by Siemens (SPPA-T3000) and the simulator is basically programmed in LabVIEW. Simulation of the solar field is done by a tool for detailed transient simulations of solar fields, called Virtual Solar Field, which was developed by the DLR. This tool is integrated to the simulator via TCP/IP connection. The plant model in LabVIEW features detailed physical models of the hydraulic network and the storage system, as well as control logics for protective functions and automatic operation modes as defined in the functional description of the test plant. Simulations validated the correct behaviour of the physical models. Measured weather data are provided as a predefined set of data with varying weather conditions (sunny or cloudy) at different seasons. The plant model can be controlled completely manually to gain experience about the behaviour of such a parabolic trough cycles.

CONTENTS

1 INTRODUCTION

At German Aerospace Center (DLR) the Institute of Solar Research is dealing with the most promising concentrating solar power (CSP) technologies, which are according to state-of-the-art, tower systems and parabolic trough systems. Parabolic troughs are the most proven CSP technology since many years. A series of nine parabolic trough power plants in the Mojave Desert of California, also called Solar Electric Generating Station I–IX (SEGS I–IX), for example, have been operating for more than 25 years and have proven the reliability and robustness of this technology. The SEGS generate about 1000 MWh net per year and achieved a decrease in cost of electricity from 30¢/kWh, in 1985 when SEGS I was built, to 14¢/kWh, in 1989 when SEGS VII was built. Still, the hurdle of very high investment costs for parabolic trough power plants remains. Further improvements of the performance, however, may put the technology onto a new level of competition where the "economy of scale" kicks in. [1] [2] [3]

The efficiency of the steam cycle, for example, is increasing with temperature and therefore it is of highest interest to identify heat transfer materials which allow to increase the steam cycle temperature. Like the nine so-called SEGS in California, commercial CSP plants with parabolic troughs are customarily using thermal oil as heat transfer fluid (HTF) and mostly utilize molten salt (MS) via heat exchangers for thermal energy storage (TES). MS is used to reduce costs and the TES volume at the same capacity compared to thermal oil. Operating temperatures of thermal oils are usually limited to about 400 °C and therefore, steam cycle temperature is not exceeding 380 °C. DLR is developing a concept to use MS as HTF for parabolic trough systems. It can be used in a temperature range of 130 °C to 580 °C (depending on salt mixture) what results in power block efficiencies of about 45% instead of 40% with thermal oil. Additional benefits of MS as HTF arise from the reduced HTF pump auxiliary load due to lower flow rates. Furthermore, and possibly most important for a renewable energy source, the concept of a two tank MS TES, as shown in Figure 1, allows decoupling the solar thermal energy generation from the electricity generation. All those benefits mentioned before are considered to result in a reduction of Levelized Costs of Electricity (LCoE) in the range of 10% to 20%. Drawbacks as the high freezing temperature of 130 °C to 200 °C (depending on salt mixture) are already considered. [4] [5] [6]

Conclusively, MS mostly implies advantages compared to thermal oil. Although MS is already established in tower systems, the widespread HTF piping, the need of flexible connections and other technical challenges when using MS for parabolic trough systems are yet to be investigated. Examples on this would include strategies for unexpected incidents or performance tests for different components. [4] [7]

1.1 Basic Concept of Molten Salt Parabolic Trough Power Plants

Figure 1 shows the basic concept of parabolic trough power plants with MS as HTF. MS is used for heat generation in the solar field (SF) as well as for TES. Therefore, compared to power plants with thermal oil as HTF, no heat exchangers are needed for the TES system. Another benefit is that heat generation in the SF is decoupled from electricity generation in the power block. Electricity can be generated according to the demand if salt is available in the hot tank. Usually a back-up system is intended to prevent solidification of the salt during periods of low solar radiation or during night-time. Many commercial parabolic trough power plants, as the SEGS, are hybridized, meaning that the back-up system is not only intended for freeze protection of the HTF but supplementing the solar output if required. Salt of the hot tank is supplied to the steam generation system (SGS) to produce steam which is typically used in a conventional Rankine cycle power block. [2] [4]

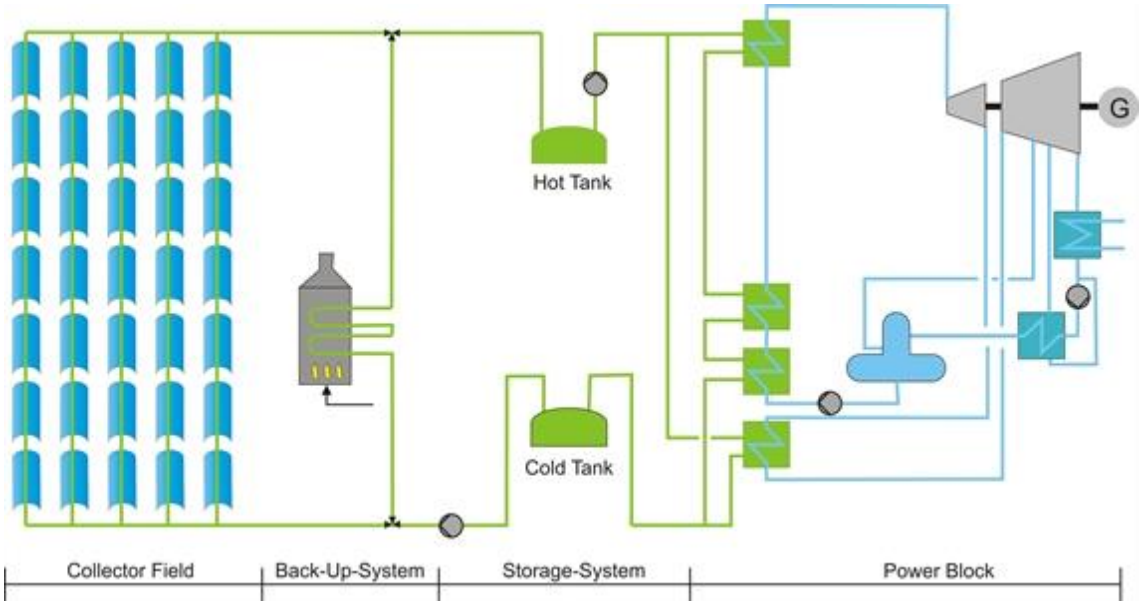

Figure 1: Basic concept of parabolic trough power plants with MS as HTF [4]

1.2 MOTIVATION OF RESEARCH

The main motivation is to address the "ten major concerns" on MS [4] [8]:

1) Ensure a filling and drainage procedure for the whole system
2) High energy consumption during operation at night to prevent solidification (parasitic load, thermal heating energy, etc.)
3) Freezing risk in different operation modes (e.g. reliability of trace heating in piping and fittings)
4) Successful blackout strategies
5) Material requirements for the high temperatures and the corrosive environment
6) Performance of the solar collectors at high temperatures (suitability of receiver, concentration factors, optical/thermal efficiency, mechanical properties)
7) Flexible connections: demonstration of function and leak tightness
8) Steam generation system: internal leakages of the heat transfer surfaces, local temperature differences between salt circuit and water circuit
9) Maintenance and operation: handling of unexpected incidents
10) Stability of the salt mixture (temporal and thermal)

In the "HPS2 – High Performance Solar 2" project, an international consortium formed by the companies eltherm production GmbH, Eskom Holdings SOC Ltd., Innogy SE, Rioglass Solar SCH, S.L., Steinmüller Engineering GmbH, TSK Flagsol GmbH, YARA GmbH & Co. KG, the Portuguese University of Évora and the DLR Institute of Solar Research is working on the demonstration of the usability of MS for parabolic trough solar power plants. The research project is a test facility initiating the Évora Molten Salt Platform (EMSP) which should provide evidence for solutions of technical challenges arising from the usage of MS as HTF. [9] [10]

1.2.1 BASIC CONCEPT OF THE TEST FACILITY

The HPS2 salt system, as shown in Figure 2, is based on the concept for commercial parabolic trough power plants with MS as HTF as described in chapter 1.1, however, does not include a conventional fossil-fuelled back-up system. Furthermore, the actual power block of the test facility is reduced as the focus of research is not on electricity generation. Details about the system schematic of the salt system, operation modes and protective measures for operation will be described in chapter 2.1.2.

The SF or collector field consists of four parabolic troughs, also called solar collector assemblies (SCAs). All SCAs are connected in series and are forming one loop with a representative length for commercial parabolic trough power plants of approximately 700 meters. The drainage system allows complete drainage and (re-)filling of the SF, the piping and the SGS. The drainage tank (DT) is positioned below ground level to enable drainage driven by gravity. It is equipped with a drainage tank pump (DP) for (re-)filling of the salt cycle and heating elements for maintenance of temperature and initial melting of the salt. [11]

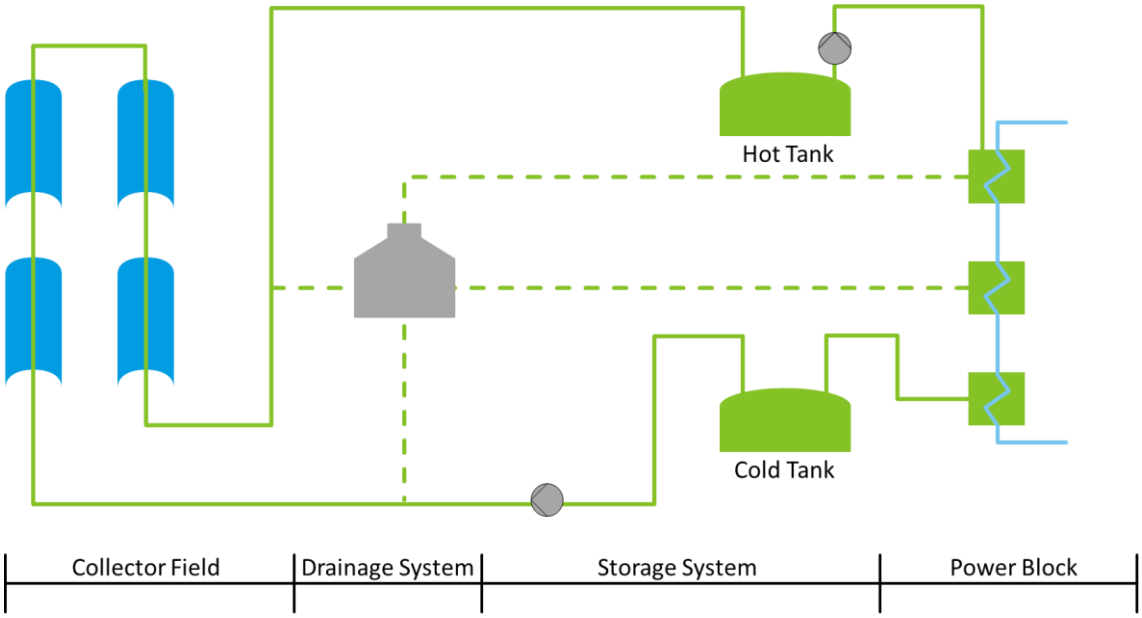

Figure 2: Basic concept of the HPS2 salt system [12]

One cold tank (CT) and one hot tank (HT) are forming the two-tank TES. Both tanks are designed to hold the entire salt volume of the system. The TES capacity is 6 MWh what corresponds to about four full-load hours of the SGS. [12] [13]

The SGS (power block) consists of a once-through Benson steam generator with a nominal power of 1.6 MWth. The steam generator is separated into three vessels where one functions as the economiser (ECO) and evaporator (EVA) and two as superheaters (SH). The steam cycle does not include a steam turbine or any system for electricity generation. The steam produced will be condensed by addition of spray, steam relaxation via valves and air-cooled condensers. [12] [13]

1.2.2 Motivation for the Development of a Simulator

The technologies and components used at the EMSP are novel and there is no experience for parabolic trough plants with MS as HTF. No standards for operation are available and, additionally, components or control systems can change regularly. The complexity of the systems is very high and complete automation of a test facility is, compared to large-scale power plants, often too expensive. Furthermore, the operating staff comes from different project partners and/or has diverse background knowledge about power plants in general and particularly about solar thermal power plants. Consequently, there exists the need to provide foregoing training to the staff with little risk of damage to the components. Therefore, development of a simulator, which enables the virtual control of the salt cycle of HPS2 and to become acquainted with the behaviour of the systems, started in 2017. [12] [14]

The main purpose of the simulator is the use during operator training. It should demonstrate the physical behaviour of the salt cycle and be controllable like the actual plant control system, which will implement a Siemens SPPA-T3000 system. [12]

Completion and improvement of the simulator was the main aim of the engagement at the Institute of Solar Research and is described in this thesis. The following chapter will describe basic operational strategies for the EMSP and will give a short overview about the state of the simulator prior to this thesis. Subsequently, the physical models and control logics implemented during this work will be described. The programming code of the simulator is not shown as that would exceed the limits. Finally, simulations done with the EMSP simulator will be shown and possible further developments as well as the context to control engineering will be discussed in a brief way.

The main physical models and control logics implemented to the simulator are dealing with:

- mutual shadowing of parabolic troughs,
- automatic operation modes of the SF and corresponding mass flow controls,
- protective control logics and
- mass flow distribution within the hydraulic networks.

2 ÉVORA MOLTEN SALT PLATFORM

The following subchapters will mainly deal with the system schematic and operation modes of the EMSP salt cycle which are important for the understanding of the physical models and control logics implemented to the simulator. Furthermore, general information on the functionality of the salt cycle will be given. Finally, the state of the EMSP simulator prior to this thesis and the concept of further developments will be described shortly.

2.1 SYSTEM SCHEMATIC AND OPERATION MODES OF THE SALT CYCLE

A simplified system schematic of the EMSP salt cycle can be seen in Figure 3. The functionalities of valves which are not part of a named branch or pipe are not of major interest for the simulator and will not be described in this thesis.

2.1.1 ABBREVIATIONS IN THE SYSTEM SCHEMATIC

SCA … solar collector assembly

SF … solar field

DP … drainage tank pump

CT … cold tank

CP … cold tank pump

HT … hot tank

HP … hot tank pump

ECO … economiser

EVA … evaporator

SH … super heater

CDI … cold distributor inlet

CDO … cold distributor outlet

CSH … cold super heater supply

HDI … hot distributor inlet

HDO … hot distributor outlet

HSH … hot super heater supply

SGS … steam generator system

The valves of the simplified system schematic are named after the corresponding pipes.

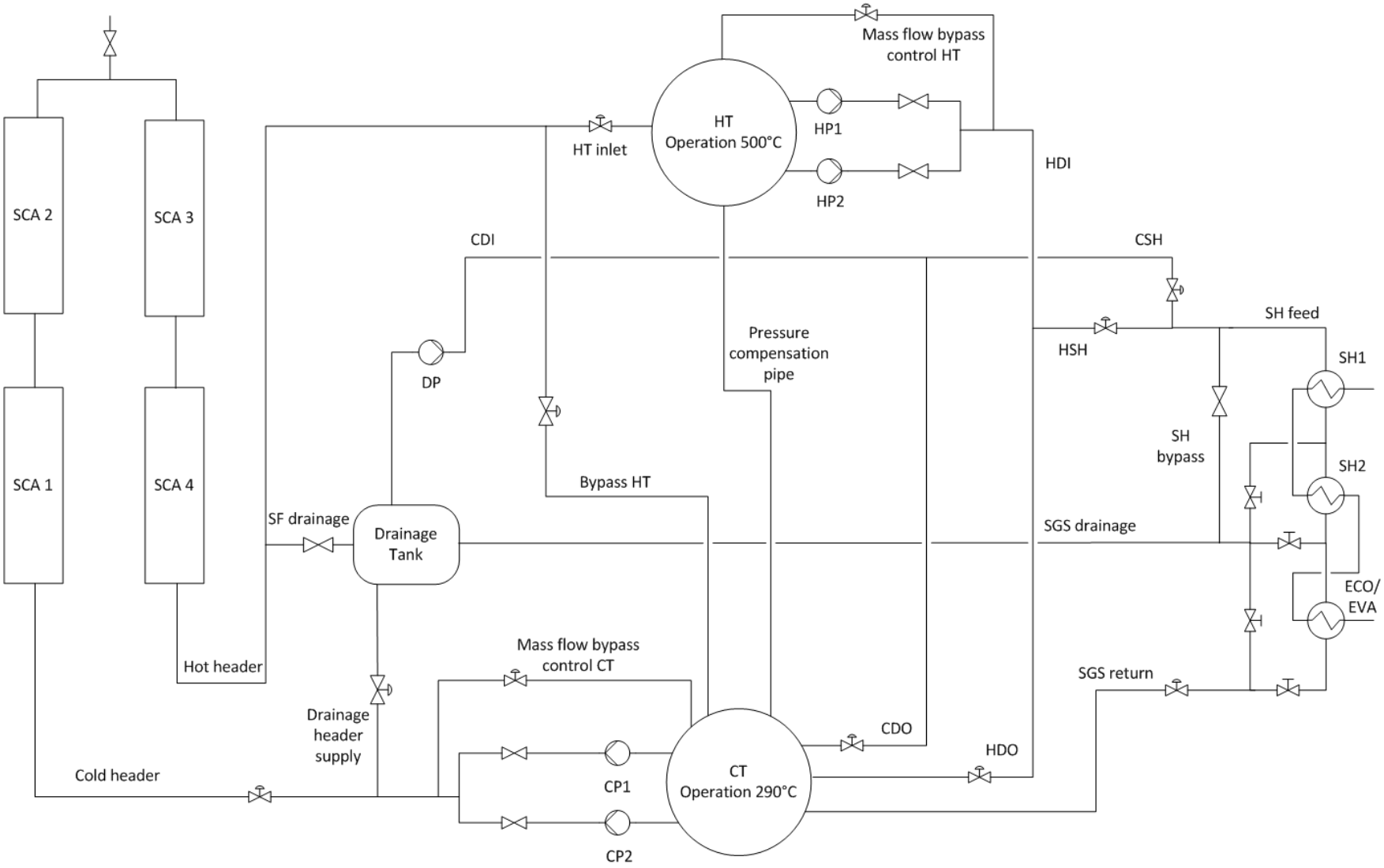

Figure 3: Simplified system schematic of the salt cycle [12]

2.1.2 SOLAR FIELD NORMAL OPERATION MODE

The normal operation mode is one of the automatic operation modes of the SF. This mode implies that the solar field is already warmed up and the outlet temperature of the SF is approximately the nominal temperature of 500 °C. Furthermore, the SCAs are focused and tracked to the movement of the sun. [15]

During this mode the MS is pumped from the CT through the cold header, the SF and the hot header into the HT. Assuming sufficient irradiation, the MS heats up when passing the receiver pipes in the focal line of the parabolic troughs (SCAs). The temperature gain depends mainly on the irradiation and the mass flow. The control unit will adjust the mass flow through the SF to stabilise the outlet temperature of the SF if fluctuations of irradiance occur. Details on the implementation of the solar field normal operation mode and the mass flow control of this mode are described in chapter 4.4. [15]

The normal operation mode is deactivated, and the shut-down mode is entered, when irradiation drops beneath a certain threshold and is not expected to reach a sufficient level within a defined period again. The shut-down sequence is not yet implemented to the simulator. [15]

2.1.3 DRAINAGE SYSTEM AND ANTI-FREEZE MODE

All pipes to and from the drainage tank are primarily designated to enable drainage of the SF, all pipes and the SGS. Additionally, the DP, the SGS drainage and SGS return pipes are intended for freeze protection in case of SGS downtimes by providing salt circulation. Furthermore, the drainage header supply allows to pump salt from the CT to the DT when MS level in the DT falls below the threshold. Level limits, which must not be exceeded, are defined for all tanks. Detailed information about the thresholds and the implementation of the tank level limits to the simulator are given in 4.6. [15]

Additional functionality for testing the SGS is provided via the cold SH supply (CSH). It allows to decrease the temperature of the MS in the SH feed by adding cold salt from the DT to the salt coming from the HT and therefore test the behaviour of the SGS if different temperature gradients are applied.

The SF shut-down mode is followed by a freeze protection mode, called SF anti-freeze mode, if irradiation is not sufficient to gain temperature. The drainage system also allows an anti-freeze mode for the SGS, however, activation of the SF anti-freeze mode and the SGS anti-freeze mode is separated as the electricity generation can be decoupled from the generation of thermal energy in the SF.

The anti-freeze mode generally means to establish a salt mass flow through pipes and equipment, which prevents the salt temperature from dropping below a minimum temperature and therefore avoid freezing of the MS. Salt from the CT and/or DT is therefore pumped in a circle. Consequently, the HT inlet valve is closed, and the Bypass HT valve is opened. MS from the hot tank will be added if temperature in the CT and/or DT drops beneath a certain threshold. For safety purposes, the minimum temperature is higher than the actual freezing temperature. This also reduces the auxiliary load during anti-freeze mode, as the viscosity increases with lower temperature (also compare chapter 3.1). The SCAs are defocused and in stow position during anti-freeze mode. [15]

2.1.4 SOLAR FIELD START-UP MODE

Usually the anti-freeze mode of the SF will be deactivated, and start-up mode of the SF will be entered, after sunrise or if sufficient irradiation is available. The SF start-up mode implies that the solar field is cooled down and all collectors are defocused. The aim of this mode is to reach the SF nominal outlet temperature and therefore the SF normal operation mode as fast as possible but still prevent dangerous plant states. The challenge is to keep the temperature gradients of the receiver pipes within a certain range and prevent thermal stresses and possible bending of the receiver pipes. The step sequence of the SF start-up mode and the mass flow control of this mode will be described in chapter 4.3.

2.1.5 MASS FLOW CONTROL

Both TES tanks are equipped with redundant pumps which are speed-controlled. Additionally, the system offers the possibility to control the flow rate with valves by adapting the hydraulic resistance through various branches of the SF or SGS, or under exceptional circumstances by using mass flow bypass control.

2.2 CONCEPT OF THE SIMULATOR

The main goal of the simulator is to allow [14]:

- Integration of a detailed solar field simulation model
- Reflection of the main operation modes and control system behaviour
- Designing a layout of the human machine interface (HMI) which is similar to the actual process control system
- Testing of process procedures of the parabolic trough test facility
- Integration of physical models of EMSP sub-systems
- Acquire experience with simulator frameworks for future test plants

As a result, LabVIEW was chosen to serve as the main simulation platform. It allows the design of a HMI, enables the simulation of physical models and control logics within LabVIEW and offers standardised connection interfaces for various simulation tools.

2.2.1 LABVIEW

LabVIEW is a programming environment developed by National Instruments with a visual programming language. It was chosen as a programming environment due to the possibilities to easily develop and adapt user interfaces. Additionally, the graphical programming approach allows visualising complex logic and offers a programming environment with a very intuitive handling. Standard connection interfaces to simulation tools like MATLAB & Simulink are available within LabVIEW. Furthermore, there exists the possibility to connect simulation tools via an OPC interface or a TCP/IP connection. [16]

Functions in LabVIEW are called VIs (Virtual Instruments). Each VI consists of a front panel, a block diagram and a connector panel, which allows data flow between VIs and allows to call VIs as sub-VIs. Like in other programming languages with functions, creating VIs for procedures often used, makes the programme clearer and easier adaptable. The front panel of an VI represents the HMI or user interface. Most usual the front panel is composed of indicators, control elements and graphics. Graphical elements, which are representing functions, are then added to the block diagram to control the front panel objects. Connecting those functions in the block diagram, then forms your code. An example of a front panel and the corresponding LabVIEW code in the block diagram is

shown in Figure 4. The front panel consists of one control element and two indicators. The block diagram shows, that the numeric entry "Numeric" is increased by "2" and the sum is then multiplied by "10". Finally, the numeric result is displayed by the indicator "Result" and the Boolean indicator "x > y?" shows if the result is greater than "50". [16]

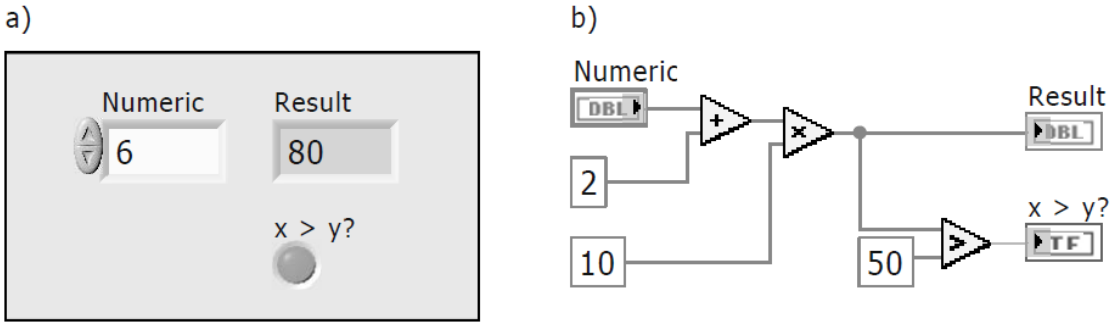

Figure 4: a) Front panel and b) graphical programming code in the block diagram [16]

LabVIEW offers many palettes, which are grouped after content, with graphical representations of functions. Programming, Mathematics, Signal Processing or Control Design & Simulation are only a few examples of palettes. Each palette then again offers groups of functions with similar tenor, like Structures (if-conditions, case structures and loops) for the Programming palette. [16]

2.2.2 State of the Simulator Prior to this Thesis

Ambient conditions are always the boundary conditions for simulations of CSP. During the development of the EMSP simulator in 2017, it was decided not to implement routines for the calculation of irradiation, track angle, et cetera to the LabVIEW programme. Therefore, there is data which need to be provided in .csv files in the simulator directory. These data include [12]:

- Direct normal irradiation (DNI)
- Factor, which includes the incidence angle modifier (IAM) and end losses, to calculate the effective irradiation g_{Eff} for each SCA,
- inclination of the sun and track angle
- ambient temperature
- wind speed

Obviously, these data strongly depend on the date and on the weather conditions during the day of simulation. For this reason, actual weather data measured at the PSA (Plataforma Solar de Almería) are provided as a predefined data set with varying weather conditions (sunny or cloudy) at different seasons. Furthermore, it is possible to provide own data in the simulator directory and use these data for the simulation of the parabolic trough test facility. The required .csv files can be generated with MATLAB.

The data handling was established and finished for the EMSP simulator. It was possible to choose the desired date of simulation beforehand, plot variables during the simulation and export the history of variables after the simulation.

The HMI of the simulator is based on pre-designs of the planned control system which will be done by Siemens (SPPA-T3000). Commercial control systems offer different panels to the operator. Therefore, the HMI of the EMSP simulator was split into four panels. The overall view or main panel showed the entire EMSP salt cycle with two control elements, both concerning the SGS. The HMI additionally consisted of three control panels [12]:

- Cold Salt Tank Panel,
- Solar Mirrors and Drainage Tank Panel and
- Hot Salt Tank Panel

Usually, it is necessary to enter the control panels to change desired values of the plant. The aim of the main panel is to indicate crucial plant parameter and give an impression over the state of the plant.

All sub-systems of the EMSP salt cycle, except the SF and the drainage system, were modelled within LabVIEW, including models for [12]:

- Auxiliary equipment, as valves, SCAs and pumps
- Thermal energy storage tanks
- Mass flow distribution of the SF cycle and the SGS cycle

A tool for detailed transient simulation of line focus solar fields, called Virtual Solar Field (VSF) was integrated to the EMSP simulator via TCP/IP connection to model the SF. Details about this tool will be outlined in chapter 2.2.3. The drainage system was not modelled prior to this thesis.

Control logics, like the automatic defocussing of a SCA when the maximum outlet temperature is exceeded, were already implemented to the simulator. Furthermore, the simulator already enabled manual control of all components implemented. The drainage tank, components and piping connected to the drainage system were not modelled prior to this thesis.

2.2.3 VIRTUAL SOLAR FIELD

The simulation of the SF is done by a tool for detailed transient simulations of solar fields, called Virtual Solar Field. This tool was developed by the DLR and is used for research in control systems engineering and operations management of line focussing solar power plants. VSF is developed in the object-oriented programming language C++. [17]

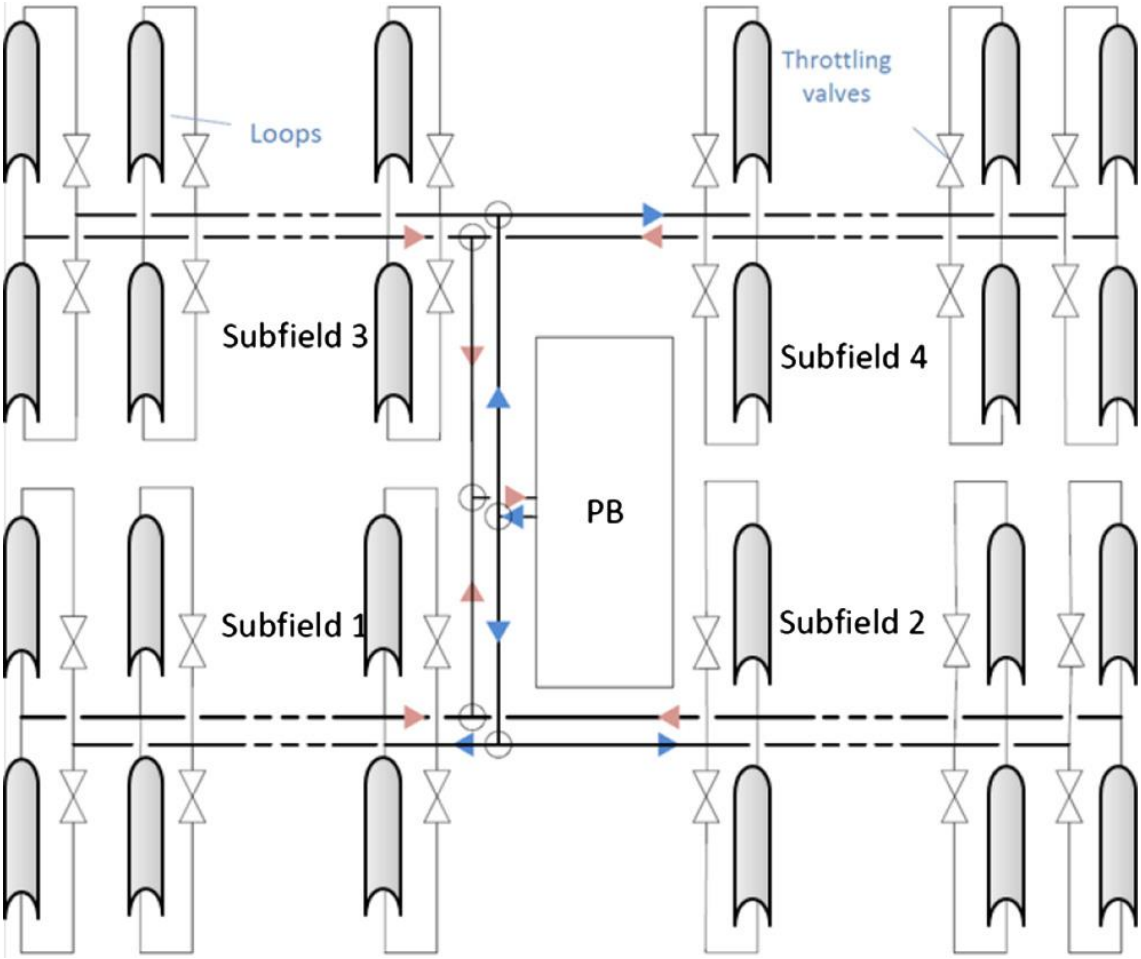

Figure 5: H-layout of a parabolic trough solar field as simulated by VSF [17] [18]

Details on the EMSP solar field model which is applied to VSF will be described in chapter 3.3.1 as there have been some changes compared to the simulator prior to this work and a new individualised model was integrated to the simulator.

Basically, VSF is a simulation tool for H-layout solar fields, as shown in Figure 5, which couples a hydraulic network solver with a thermal solver. Therefore, it considers hydraulic resistances to calculate the mass flow distribution in the solar field and thermal gains and losses to compute the temperatures in all pipes and receivers. The tool allows the representation of auxiliary equipment, like pumps or valves, enables the use of irradiation maps and includes control parameters which are provided locally for each SCA or globally for HTF pumps and valves. All pipes and loops are discretised along the axis of fluid flow. The fluid flow is assumed to be one-dimensional. [18] [19]

2.2.4 FURTHER DEVELOPMENTS OF THE SIMULATOR

Development of the simulator as described in 2.2.2 is outlined in [12]. This chapter describes constraints of the simulator prior to this thesis and improvements which were intended to be implemented during my engagement at DLR / Institute of Solar Research.

In principle, the simulator should not include features which are not available in the actual control system or which definition is not finalised in the functional description, as during training, the operators should not get a wrong impression of the control system features. Therefore, further developments mainly deal with:

- Physically accurate characterisation of sub-systems and components
- Operation modes and mass flow controllers
- Protective control logics

The main goal of all further developments was to characterise the salt cycle as accurate as possible with reasonable effort and to establish all automatic operation modes for the SF, so that a simulation over the day without manual control would be possible (assuming fair ambient conditions or boundary conditions).

Manual simulation for the time around sunrise showed, that mutual shadowing of the parabolic troughs was not considered yet, however, it strongly affects the SF start-up, when heat generation is started in the morning, and the operation before sunset.

As described in 2.2.2, the purpose of the main panel is to indicate crucial plant parameter and give an impression over the state of the plant. Control elements are usually only available in sub-panels or control panels. Additionally, considering that the simulator is based on pre-designs of the control system which will be applied to the real plant, there existed the need of implementing a control panel for the SGS.

Prior to this thesis, the drainage tank and connection pipes were not modelled, resulting in a salt sink when directing salt to the drainage tank. Therefore, applying different temperature gradients to the SGS, as described in chapter 2.1.3, was not possible.

Additionally, mass flow distribution within pipework was virtually distributed proportional to the valve openings and was not considering hydraulic resistances.

The process control system of the plant will also allow to operate the solar field in automatic modes which were not implemented to the simulator.

3 PHYSICAL MODELS

This chapter deals with physical models which were implemented during my engagement at DLR. Different VIs, as outlined in 3.1, were introduced to make existing code more comprehensible. Chapter 3.2 describes the drainage tank model, which is consistent with the TES model as in [12]. Mass flow distribution of the SF cycle, as outlined in 3.3, is evaluated by VSF, while mass flow distribution of the SGS cycle is modelled within LabVIEW. Chapter 3.4 describes the methods to model hydraulic networks. Finally, chapter 3.5 explains modelling mutual trough shading at low sun elevation.

3.1 CALCULATION OF THERMOPHYSICAL PROPERTIES

The HTF of the EMSP is a ternary salt mixture produced by YARA. As thermophysical properties of the used molten salt are required for various models in the simulator, there was the need to programme a central VI which calculates the thermophysical properties as a function of temperature. The correlations for the specific heat capacity c_p, the density ρ and the dynamic viscosity η of a similar ternary molten salt mixture were published in 2011 by Siegel in [20] and are formulated as follows:

$$c_p = -0.000325 \cdot \vartheta + 1.539\,, \tag{3.1}$$

$$\rho = -0.827 \cdot \vartheta + 2240\,, \tag{3.2}$$

$$\eta = 1372144.977 \cdot \vartheta^{-3.36406}\,, \tag{3.3}$$

with

$$c_p\ in\ \frac{kJ}{kg \cdot K}\,,$$

$$\eta\ in\ Pa \cdot s\,,$$

$$\rho\ in\ \frac{kg}{m^3}\,,$$

and the temperature

$$\vartheta\ in\ °C.$$

In addition, the enthalpy is crucial to the formulation of energy balance equations.

$$\int_{\vartheta_0}^{\vartheta_1} dh = \int_{\vartheta_0}^{\vartheta_1} c_p \cdot d\vartheta = \int_{\vartheta_0}^{\vartheta_1} (-0.000325 \cdot \vartheta + 1.539) \cdot d\vartheta \tag{3.4}$$

The integral of dh is equal to the integral of $d\vartheta$ over c_p. Using the correlation for the specific heat capacity, shown in (3.1), the equation can be written as:

$$h(\vartheta_1) - h(\vartheta_0) = -\frac{1}{2} \cdot 0.000325 \cdot (\vartheta_1^2 - \vartheta_0^2) + 1.539 \cdot (\vartheta_1 - \vartheta_0)\,. \tag{3.5}$$

Defining the boundary conditions as:

$$h(\vartheta_0) = 0\,\frac{kJ}{kg}\,, \tag{3.6}$$

$$\vartheta_0 = 0°C \tag{3.7}$$

and applying the boundaries gives:

$$h(\vartheta_1) = -\frac{1}{2} \cdot 0.000325 \cdot \vartheta_1^2 + 1.539 \cdot \vartheta_1\,. \tag{3.8}$$

As a result, the enthalpy h can be written as a function of the temperature ϑ:

$$h = a \cdot \vartheta^2 + b \cdot \vartheta\,. \tag{3.9}$$

Back converting the enthalpy h to the corresponding temperature ϑ can be done by rearranging equation (3.9) to:

$$0 = a \cdot \vartheta^2 + b \cdot \vartheta - h\,. \tag{3.10}$$

Therefore,

$$\vartheta_{1,2} = \frac{-b \pm \sqrt{b^2 - 4ah}}{2a}\,. \tag{3.11}$$

To meet the boundary conditions defined in (3.6) and (3.7), the only reasonable result can be:

$$\vartheta = \frac{-b + \sqrt{b^2 - 4ah}}{2a}\,, \tag{3.12}$$

with

$$a = -\frac{1}{2} \cdot 0.000325$$

and

$$b = 1.539\,.$$

The VI for computation of the thermophysical properties needed is using equations (3.1) to (3.12) for the calculation of the specific heat capacity c_p, the density ρ, the dynamic viscosity η and the specific enthalpy h as a function of the temperature ϑ. Additionally, it gives the temperature ϑ as a function of the enthalpy h. The VI is crucial to many physical models which are described in the following subchapters.

3.2 DRAINAGE TANK MODEL

The drainage tank balance equations are consistent with the model for the TES tanks as described in [12] and will be outlined shortly in this chapter. The drainage tank can be described as a horizontal cylindrical tank with a diameter of $d_{DT} = 1.8\,m$. Therefore, volume changes are not linear, and the calculation of the MS level cannot be done analytically. A polynomial function of the fifth order is used to approximate the drainage tank salt level l_{DT} as a function of the MS volume V:

$$l_{DT} = 1.75 \cdot 10^{-5} \cdot V^5 - 6.22 \cdot 10^{-4} \cdot V^4 + 8.38 \cdot 10^{-3} \cdot V^3 - 5.29 \cdot 10^{-2} \cdot V^2 + 0.257 \cdot V\,. \tag{3.13}$$

Conversion from mass to volume and vice versa is done using the VI for the calculation of thermophysical properties, as described in chapter 3.1.

3.2.1 BALANCE EQUATIONS

The tanks are modelled using continuity and energy conservation equations. [21]

The continuity equation includes the salt mass within the tank m_{tank} as well as all mass flow rates into the tank $\dot{m}_{in}$ and out of the tank $\dot{m}_{out}$. The temporally discretised equation can be formulated as:

$$m_{tank}^{t} = m_{tank}^{t-\Delta t} + \dot{m}_{in}^{t-\Delta t} \cdot \Delta t - \dot{m}_{out}^{t-\Delta t} \cdot \Delta t\,, \tag{3.14}$$

where the superscript t describes the current state and Δt is the time step.

The energy conservation equation is used for the evaluation of the salt temperature in the tank and can basically be described like the continuity equation (3.14) by multiplying all terms with the corresponding specific enthalpy h of the salt mass or salt mass flow. Additionally, the thermal losses of the tank $\dot{Q}_{tank}$ need to be considered. Moreover, all tanks are equipped with electrical heating elements, which thermal input $P_{aux,el}$

as well contributes to the energy conservation equation. The discretised equation can be written as:

$$h_{tank}^{t} = \frac{1}{m_{tank}^{t}} \cdot (m_{tank}^{t-\Delta t} \cdot h_{tank}^{t-\Delta t} + \dot{m}_{in}^{t-\Delta t} \cdot h_{in}^{t-\Delta t} \cdot \Delta t \\ -\dot{m}_{out}^{t-\Delta t} \cdot h_{out}^{t-\Delta t} \cdot \Delta t - \dot{Q}_{tank}^{t-\Delta t} \cdot \Delta t \cdot 10^{-3} + P_{aux,el}^{t-\Delta t} \cdot \Delta t \cdot 10^{-3}) \,, \tag{3.15}$$

with

$$h \; in \; \frac{kJ}{kg},$$

$$\dot{Q} \; in \; W$$

and

$$P \; in \; W.$$

Heating elements are not yet implemented to the simulator and therefore the thermal input $P_{aux,el}$ is set to zero. A value for the thermal losses of the tanks need to be entered at the beginning of each simulation. The default value is set to

$$\dot{Q}_{tank} = 1000 \; W.$$

The thermal losses are assumed to be constant. Furthermore, thermal stratification is neglected.

3.3 Mass Flow Distribution of the Solar Field Cycle

The mass flow, which is driven by the pressure head of the cold pumps, distributes according to the valve openings and therefore according to the total hydraulic resistances of the mass flow bypass control CT branch, the drainage header supply branch and the cold header branch. As VSF is the tool of choice to model the SF, it was decided to change the individualized VSF-model so that it is modelling all branches mentioned before. The individualized VSF-model will be described in the following subchapter.

3.3.1 Individualised VSF-Model

A simplified system schematic according to the individualised VSF-model can be seen in Figure 6. It shows the three branches of possible fluid flow mentioned in 3.3. Like the pressure $p2$, the pressure of each branch outlet is assumed to be ambient pressure, as the TES tanks are atmospheric tanks.

This definition together with the current valve openings of each branch and the inlet pressure $p1$ defines the hydraulic network and enables the calculation of the mass flow distribution. The inlet pressure $p1$ results from the mass flow control which is described for each operation mode in chapter 4. The inlet temperature of the HTF is assumed to be equal to the temperature in the CT. The valve openings are controlled by the operator using the control elements of the HMI. The ambient temperature as well as the deviation angles and the effective irradiation g_{Eff} for each SCA are needed for the energy balance equations to calculate the thermal losses or gains of the pipes and the SCAs. The deviation angle describes the angle between the actual SCA angle and the optimum track angle to the sun.

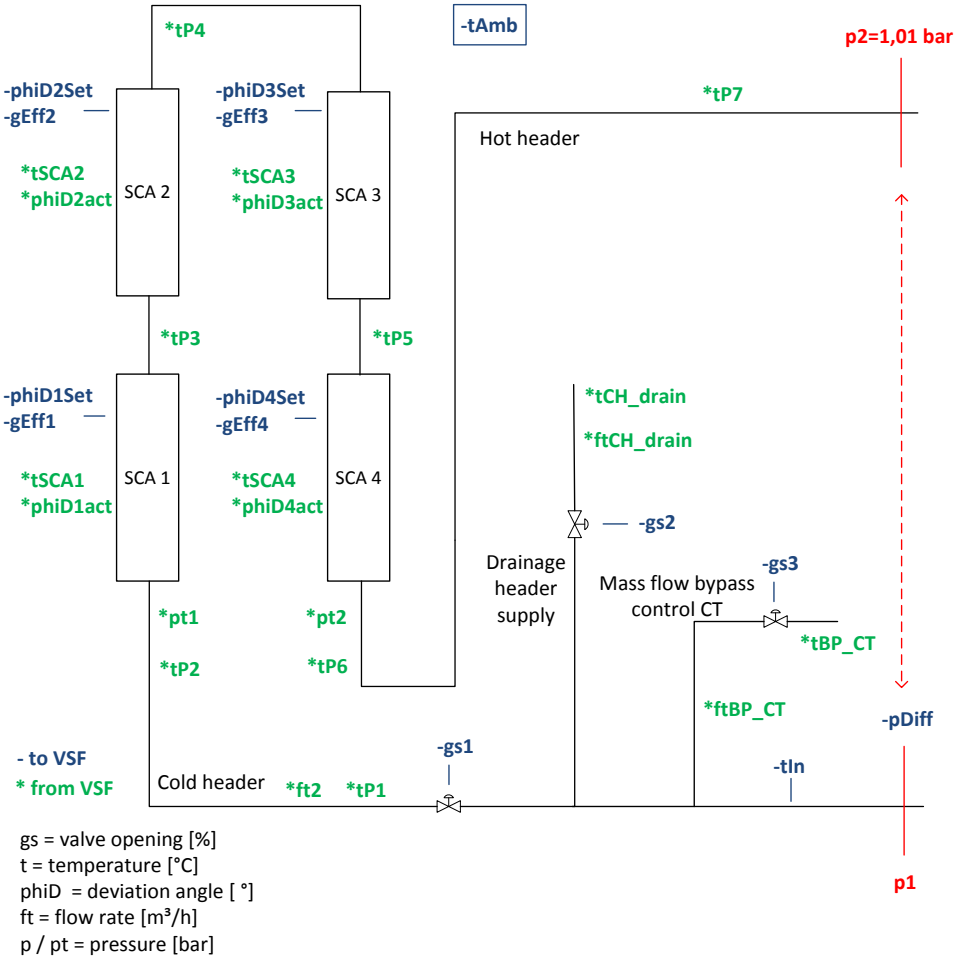

Figure 6: Individualised VSF-model of the solar field cycle (after [12])

3.4 Mass Flow Distribution of the Steam Generator Cycle

The mass flow distribution of the SGS cycle is simulated within LabVIEW. The methods are consistent with the methods used in VSF and will be described in the following subchapters. The challenge of this hydraulic network is, that backflow can occur under certain operational circumstances. Case structures are used to account for these backflow conditions.

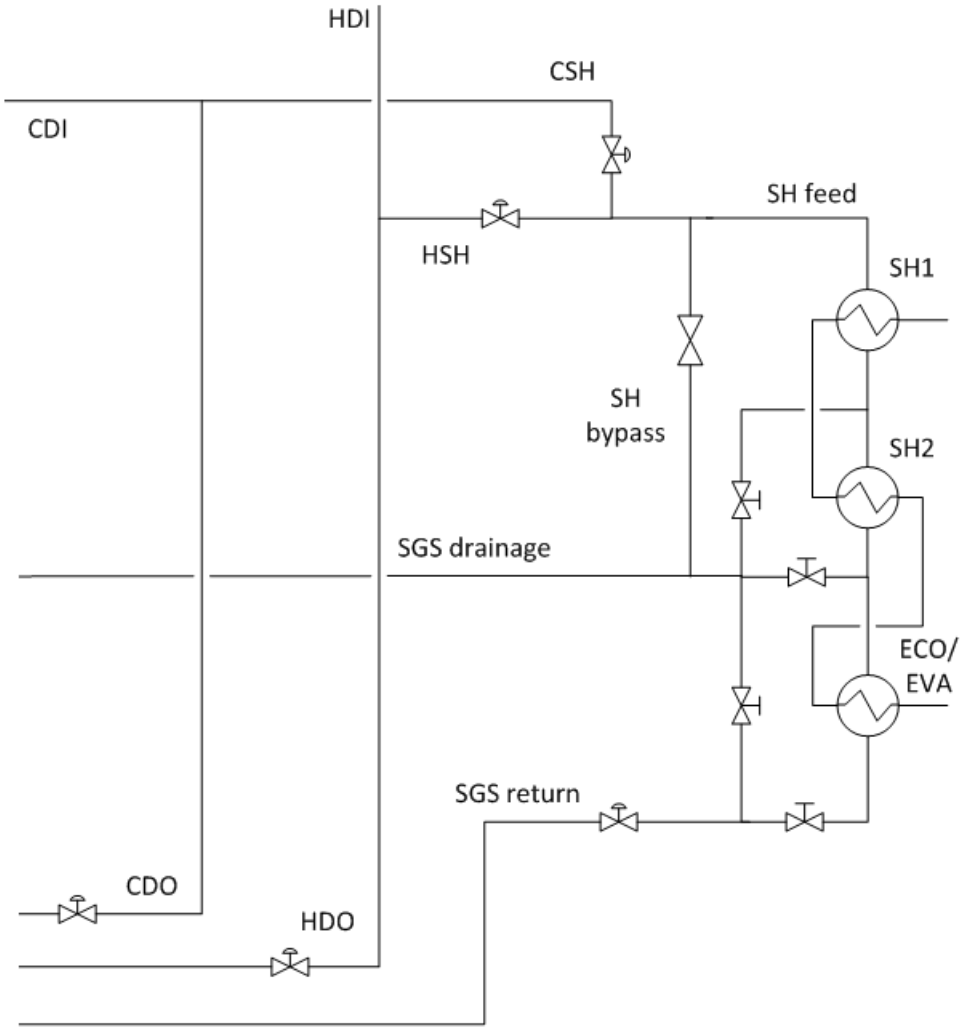

Figure 7: Simplified system schematic of the SGS cycle

The simplified steam generator cycle can be seen in Figure 7. The mass flow bypass control HT branch, as shown in Figure 3, is not modelled. The cycle includes two potential MS sources, the DT and the HT. The HT pumps are each coupled with a solenoid valve which is closed if the corresponding pump is not in operation (see Figure 3). The

DP, however, is not equipped with such a valve, what results in a possible backflow into the DT if the DP is turned off but the CSH valve is opened. Additionally, the fact that the DT is positioned below ground level intensifies this backflow conditions and theoretically allows backflow even if no pump of the SGS cycle is in operation. A control logic, which prevents backflow through the DP into the DT is not scheduled. However, a warning, which is not yet implemented to the simulator, will appear in case of backflow through the DP. The model of this hydraulic network must exclude backflow through the CDO and the HDO branch. Without any pump being in operation, gravitational force would theoretically lead to backflow through those two branches. Since the CDO and HDO outlets are both not immersed in MS, backflow is physically not possible.

The case structures to prevent certain backflow conditions are, like programming code in general, not shown and described in more detail in this thesis.

3.4.1 Mixing Temperature of Salt Mass Flows

With the DP and a HT pump in regular operation, salt from the DT and from the HT is mixed after the HSH and CSH outlet (see Figure 7). Both salt mass flows usually provide MS with different temperatures. Therefore, calculation of the mixing temperature is necessary. Like in chapter 3.2.1, the energy balance equation is used:

$$h_{SHfeed} = \frac{1}{\dot{m}_{CSH} + \dot{m}_{HSH}} \cdot (\dot{m}_{CSH} \cdot h_{CSH} + \dot{m}_{HSH} \cdot h_{HSH}) \,. \tag{3.16}$$

Converting temperatures to enthalpies h and vice versa is done using the VI for the calculation of thermophysical properties, as described in chapter 3.1. Thermal losses are currently not considered in the SGS cycle, as the discretisation of the hydraulic network would require an externally programmed tool like VSF.

3.4.2 Hydraulic Network of the Steam Generator Cycle

Figure 8 shows a simplified hydraulic network of the SGS cycle, displayed like an electric circuit. In the following the hydraulic analogies of Kirchhoff´s current and voltage law will be applied to set up a system of equations which allows the evaluation of the mass flow distribution in this hydraulic network. This method is, among others, used to model water supply pipe networks as described in [22].

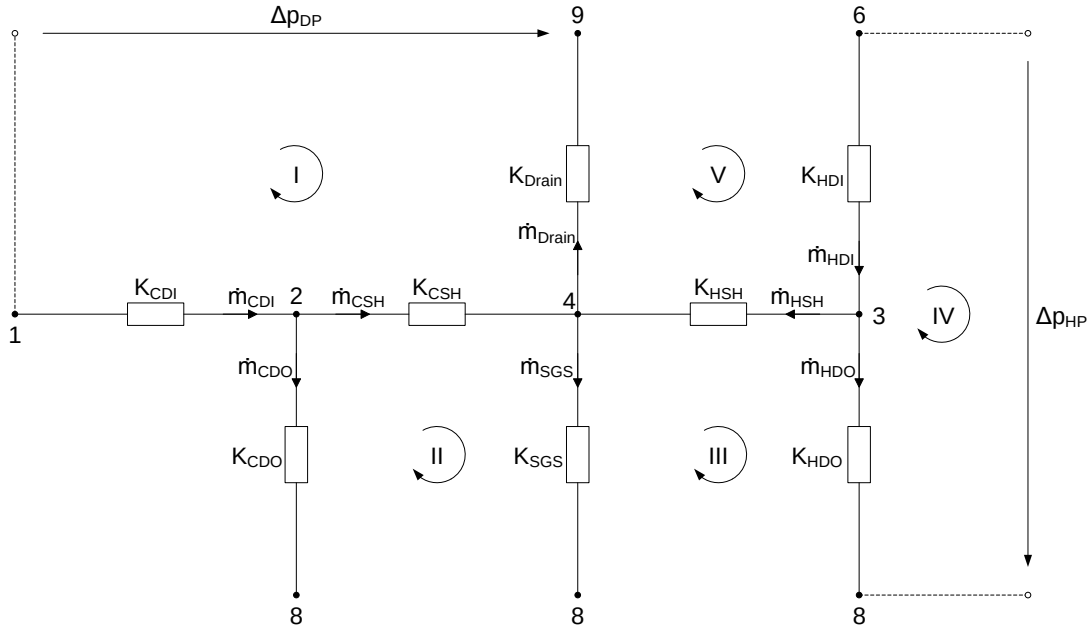

Figure 8: Simplified hydraulic network of the SGS cycle

K … Hydraulic resistance

$\dot{m}$ … Mass flow

Δp … Pressure difference

$_{CDI}$ … Cold distributor inlet

$_{CDO}$ … Cold distributor outlet

$_{CSH}$ … Cold superheater supply

$_{HDI}$ … Hot distributor inlet

$_{HDO}$ … Hot distributor outlet

$_{HSH}$ … Hot superheater supply

$_{SGS}$ … Steam generator system

$_{SHFeed}$ … Superheater feed

$_{EVAout}$ … Evaporator outlet

$_{Drain}$ … Drainage pipe

$_{DP}$ … Drainage tank pump

$_{HP}$ … Hot tank pump

According to the hydraulic analogy of Kirchhoff´s current law, the fluid flows of all pipes connected to a node must satisfy the continuity equation [19] [22]. Therefore, the equations for Node 2, 3 and 4 in Figure 8 can be written as:

Node 2: $$\dot{m}_{CDI} - \dot{m}_{CDO} - \dot{m}_{CSH} = 0 \tag{3.17}$$

Node 3: $$\dot{m}_{HDI} - \dot{m}_{HDO} - \dot{m}_{HSH} = 0 \tag{3.18}$$

Node 4: $$\dot{m}_{CSH} + \dot{m}_{HSH} - \dot{m}_{SGS} - \dot{m}_{Drain} = 0 \tag{3.19}$$

Kirchhoff´s voltage law applied to fluid flow, describes that the pressure drops around a hydraulic loop are equal to zero. Pumps are acting as sources of pressure differences whereby valves, pipes and bends are resulting in pressure losses. [19] [22]

Consequently, the equations for the five loops in Figure 8 are formulated as follows:

Loop I: $$\Delta p_{DP} - K_{Drain} \cdot \dot{m}_{Drain} \cdot |\dot{m}_{Drain}| - K_{CSH} \cdot \dot{m}_{CSH} \cdot |\dot{m}_{CSH}| - K_{CDI} \cdot \dot{m}_{CDI} \cdot |\dot{m}_{CDI}| + \rho \cdot g \cdot (h_1 - h_9) = 0 \tag{3.20}$$

Loop II: $$-K_{CDO} \cdot \dot{m}_{CDO} \cdot |\dot{m}_{CDO}| + K_{CSH} \cdot \dot{m}_{CSH} \cdot |\dot{m}_{CSH}| + K_{SGS} \cdot \dot{m}_{SGS} \cdot |\dot{m}_{SGS}| = 0 \tag{3.21}$$

Loop III: $$-K_{SGS} \cdot \dot{m}_{SGS} \cdot |\dot{m}_{SGS}| - K_{HSH} \cdot \dot{m}_{HSH} \cdot |\dot{m}_{HSH}| + K_{HDO} \cdot \dot{m}_{HDO} \cdot |\dot{m}_{HDO}| = 0 \tag{3.22}$$

Loop IV: $$\Delta p_{HP} - K_{HDO} \cdot \dot{m}_{HDO} \cdot |\dot{m}_{HDO}| - K_{HDI} \cdot \dot{m}_{HDI} \cdot |\dot{m}_{HDI}| + \rho \cdot g \cdot (h_6 - h_8) = 0 \tag{3.23}$$

Loop V: $$-\Delta p_{HP} + K_{HDI} \cdot \dot{m}_{HDI} \cdot |\dot{m}_{HDI}| + K_{HSH} \cdot \dot{m}_{HSH} \cdot |\dot{m}_{HSH}| + K_{Drain} \cdot \dot{m}_{Drain} \cdot |\dot{m}_{Drain}| + \rho \cdot g \cdot (h_9 - h_6) = 0 \tag{3.24}$$

Pressure drops of each branch are expressed in the form $\Delta p = K \cdot \dot{m}^2$, where K is the total hydraulic resistance and $\dot{m}$ is the mass flow.

To account for the direction of mass flow, $\dot{m} \cdot |\dot{m}|$ is used instead of $\dot{m}^2$. Fluid flow in clock-wise direction, as shown in Figure 8 by the loop arrows, is considered as positive pressure drop, fluid flow in counter-clock-wise direction is indicated as negative pres-

sure drop. Pumps and changes in height h between nodes, which are given in Table 1, are sources of pressure difference. [19]

Pressure losses are the result of friction or surface resistance due to mass flow through pipes and form resistance losses due to bends, valves, elbows, et cetera. The total hydraulic resistance K of a branch is derived from the sum of all hydraulic resistances incorporated in a branch. Table 1 shows the data needed for the evaluation of the total hydraulic resistances. [22]

The inner diameter of all pipes is 77.92 mm (ND 2 inch). All valves, however, are the size of two inches. Form resistance losses due to reducers, pipe entrances or outlets are neglected.

The pressure drop through the Benson steam generator is assumed to be a function of mass flow only. Calculated data are available from the manufacturer.

Table 1: List of branches with the corresponding data for the calculation of the hydraulic resistances

Branch/Node	Length/height in mm	Bends	Valve
K_{HDI}	5397	4 x 90°	01WTA42AA001
K_{HDO}	6596	4 x 90°	01WTA50AA101
K_{HSH}	11578	3 x 90°	01WTA51AA101
K_{CDI}	3494	3 x 90°	-
K_{CDO}	29796	11 x 90°	01WTE10AA101
K_{CSH}	9247	3 x 90°	01WTE11AA101
K_{Drain}	8672	5 x 90°	01WTA51AA401
$Node\ 1$	67	-	-
$Node\ 6$	6866	-	-
$Node\ 8$	5910	-	-
$Node\ 9$	0	-	-
K_{SGS}:			
K_{SHFeed}	8531	2 x 90°	-
K_{EVAout}	21318	5 x 90°	01WTA70AA101

3.4.3 HYDRAULIC RESISTANCE OF PIPES, BENDS AND VALVES

According to the Darcy-Weisbach relation, frictional head losses h_f due to pipe flow can be calculated with:

$$h_f = f \cdot \frac{L}{D_{in}} \cdot \frac{v^2}{2 \cdot g} \,, \tag{3.25}$$

where v is the mean flow velocity, $\frac{L}{D_{in}}$ is the pipe length divided by the inner pipe diameter, f is the Darcy friction factor and g is the gravitational acceleration. [19]

Using conserved quantities instead of the frictional head loss and the velocity, as described in [19], results in equation (3.28). The pressure drop is evaluated with:

$$\Delta p = \rho \cdot g \cdot h_f \tag{3.26}$$

and the velocity through a pipe with a cross sectional area A_{in} can be written as:

$$v = \frac{\dot{m}}{A_{in} \cdot \rho} \,. \tag{3.27}$$

Therefore, the form $\Delta p = K_p \cdot \dot{m}^2$, as shown in equations (3.20) to (3.24) can be used. The total hydraulic resistance of a pipe K_p is calculated as:

$$K_p = \frac{L}{D_{in}} \cdot \frac{f}{2 \cdot A_{in}^2 \cdot \rho} \,. \tag{3.28}$$

The Darcy friction factor can be evaluated using the correlation for all fluid-flow regimes after Churchill [23]:

$$f = 8 \cdot \left[\left(\frac{8}{Re} \right)^{12} + \frac{1}{(A + B)^{\frac{3}{2}}} \right]^{\frac{1}{12}} \,, \tag{3.29}$$

with

$$A = \left[2.457 \cdot \ln \frac{1}{\left(\frac{7}{Re} \right)^{0.9} + \frac{0.27 \cdot \varepsilon}{D_{in}}} \right]^{16}$$

and

$$B = \left(\frac{37{,}530}{Re} \right)^{16} \,.$$

Here, the variable ε describes the effective roughness of the pipe, which is assumed to be $0.05\,mm$ for commercial new steel pipes [24]. The calculation of the Reynolds number is done by a separate VI. It is using the VI described in 3.1 for the evaluation of the dynamic viscosity η and the density ρ and calculates the Reynolds number as:

$$Re = \frac{v \cdot D_{in} \cdot \rho}{\eta} \,. \tag{3.30}$$

The calculation of valve pressure drops is done as described in [19].
The valve flow coefficient K_V, which is given in m^3/h, characterises industrial valves and is defined as the volume flow rate of water through the valve at 1 bar differential pressure across the valve. It is a function of the percentage of valve opening. [19]

The volume flow rate of a fluid through a valve in m^3/h can be calculated with:

$$\dot{V} = \frac{1}{\sqrt{\frac{1}{\Delta p_V} \cdot \frac{\rho}{\rho_W}}} \cdot K_V \,, \tag{3.31}$$

where ρ_W is the reference density of water which is equal to 1000 kg/m^3 and the pressure drop is given in bar. Rearranging equation (3.31) gives the pressure drop across a valve as a function of volume flow:

$$\Delta p_V = \frac{1}{K_V^2} \cdot \frac{\rho}{\rho_W} \cdot \dot{V}^2 \,. \tag{3.32}$$

Since the volume flow rate $\dot{V}$ is:

$$\dot{V} = \frac{\dot{m}}{\rho} \,, \tag{3.33}$$

equation (3.32) can be brought into the form $\Delta p_V = K_{V,SI} \cdot \dot{m}^2$. Additionally, applying SI-units gives:

$$\Delta p_V = \frac{10^5 \cdot 3600^2}{K_V^2 \cdot \rho_W \cdot \rho} \cdot \dot{m}^2 \,. \tag{3.34}$$

Therefore, the hydraulic resistance $K_{V,SI}$ for valves is calculated as:

$$K_{V,SI} = \frac{10^5 \cdot 3600^2}{K_V^2 \cdot \rho_W \cdot \rho} \,. \tag{3.35}$$

An approximation for the hydraulic resistance of 90° pipe bends in turbulent flow is given in [24] as:

$$K_{bend} \approx 0.388 \cdot \alpha \cdot \left(\frac{R}{d}\right)^{0.84} \cdot Re^{-0,17} , \tag{3.36}$$

with

$$\alpha = 0.95 + 4.42 \cdot \left(\frac{R}{d}\right)^{-1.96} ,$$

where d is the pipe diameter and R is the curvature radius.

According to Table 1 the hydraulic resistances of the branches are:

$$K_{CSH} = 3 \cdot K_{bend} + K_{p,CSH} + K_{V,SI,CSH} , \tag{3.37}$$

$$K_{CDO} = 11 \cdot K_{bend} + K_{p,CDO} + K_{V,SI,CDO} , \tag{3.38}$$

$$K_{CDI} = 3 \cdot K_{bend} + K_{p,CDI} , \tag{3.39}$$

$$K_{HSH} = 3 \cdot K_{bend} + K_{p,HSH} + K_{V,SI,HSH} , \tag{3.40}$$

$$K_{HDO} = 4 \cdot K_{bend} + K_{p,HDO} + K_{V,SI,HDO} , \tag{3.41}$$

$$K_{HDI} = 4 \cdot K_{bend} + K_{p,HDI} + K_{V,SI,HDI} , \tag{3.42}$$

$$K_{Drain} = 5 \cdot K_{bend} + K_{p,Drain} + K_{V,SI,Drain} , \tag{3.43}$$

$$K_{SGS} \cdot \dot{m}_{SGS}^2 = \left(7 \cdot K_{bend} + K_{p,SHFeed} + K_{p,EVAout} + K_{V,SI,EVAout}\right) \cdot \dot{m}_{SGS}^2 + 3.0644 \cdot \dot{m}_{SGS}^2 - 0.2034 \cdot \dot{m}_{SGS} + 2.2712 . \tag{3.44}$$

Equation (3.44) results from the hydraulic resistance of the superheater feed and the evaporator outlet as well as the correlation for the pressure drop through the Benson steam generator.

3.4.4 NEWTON-RAPHSON METHOD

Equations (3.17) to (3.24) form the system of eight equations that needs to be solved. The calculation of hydraulic resistances was described in the last chapter. The differential pump pressures result from the control panels of the simulator as a function of pump

rotational speed. Therefore, there is a set of eight equations with eight mass flow rates as unknown variables. The system of equations, however, is nonlinear and requires an iterative approach to solve it. The Newton-Raphson method is a numerical approach for solving systems of nonlinear equations. [19] [22]

The procedure to solve a set of non-linear equations using Newton-Raphson method is taken from [22].

The eight equations F_1 (3.17) to F_8 (3.24) are functions of the unknown mass flow rates $\dot{m}_1$ to $\dot{m}_8$ and need to be solved for those mass flow rates. Bringing the set of equations into matrix form and using Newton-Raphson method results in the matrix equation:

$$\Delta\dot{m}_i = -\left[\frac{\partial F_n}{\partial \dot{m}_i}\right]^{-1} \cdot F_n \,, \tag{3.45}$$

where $\left[\frac{\partial F_n}{\partial \dot{m}_i}\right]$ and F_n represent the values of the Jacobian matrix and the left-hand side of equations F_1 (3.17) to F_8 (3.24) in vector form, respectively. A set of initial mass flow rates, which satisfies the continuity equations, needs to be defined as an initial guess or starting point to enable calculating these values. The result is the vector $\Delta\dot{m}_i$ which gives correction values for the mass flow rates. Those correction values are improving the initial guess of mass flow rates:

$$\begin{bmatrix}\dot{m}_1\\ \dot{m}_2\\ \dot{m}_3\\ \dot{m}_4\\ \dot{m}_5\\ \dot{m}_6\\ \dot{m}_7\\ \dot{m}_8\end{bmatrix} = \begin{bmatrix}\dot{m}_1\\ \dot{m}_2\\ \dot{m}_3\\ \dot{m}_4\\ \dot{m}_5\\ \dot{m}_6\\ \dot{m}_7\\ \dot{m}_8\end{bmatrix} + \begin{bmatrix}\Delta\dot{m}_1\\ \Delta\dot{m}_2\\ \Delta\dot{m}_3\\ \Delta\dot{m}_4\\ \Delta\dot{m}_5\\ \Delta\dot{m}_6\\ \Delta\dot{m}_7\\ \Delta\dot{m}_8\end{bmatrix}, \tag{3.46}$$

and allow iteration, which takes place until all the correction values $\Delta\dot{m}_i$ are below a very small threshold. During simulation the initial guess is equal to the mass flow of the previous time step. Therefore, convergence usually occurs within several iterations, however, inverting the Jacobian matrix can be very time consuming for large hydraulic networks. [19] [22]

3.5 IMPLEMENTATION OF MUTUAL TROUGH SHADING

Modelling mutual trough shading of a parabolic trough with the aperture width w can be described by Figure 9. A factor η_{shadow} which is defined as $\eta_{shadow} = \frac{w_{unshaded}}{w}$ is introduced and describes the percentage of unshaded aperture width:

$$\eta_{shadow} = \cos(\rho) * \frac{L_{space}}{w} \; . \tag{3.47}$$

The cosine of the zenith angle $\cos(\rho)$ is equal to $\frac{w_{unshaded}}{L_{space}}$. Multiplication with the fraction of the row distance L_{space} divided by the aperture width of the parabolic trough w allows to cancel L_{space} and finally gives the percentage of unshaded aperture width η_{shadow}. The result needs to be bounded with a minimum value of zero and a maximum value of one.

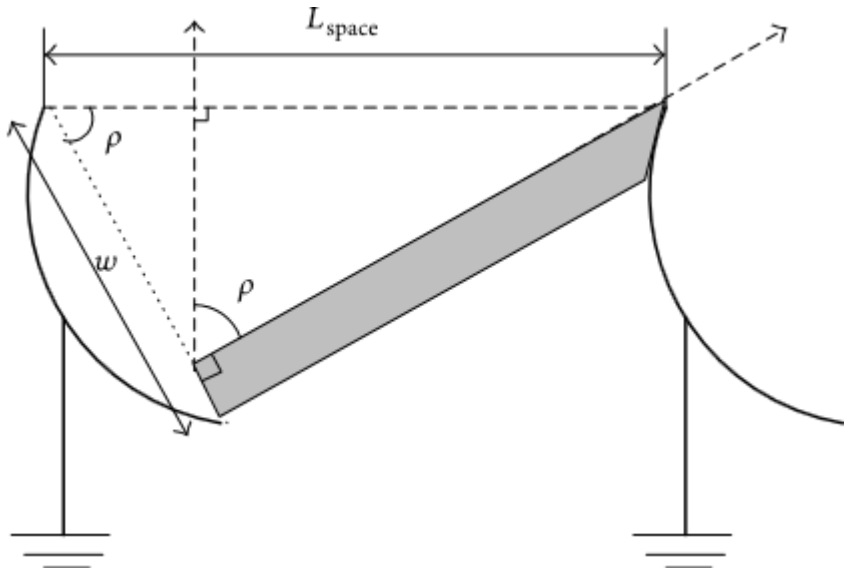

Figure 9: Mutual trough shading of adjacent SCAs [25]

The model is only considering the zenith angle and assumes a solar azimuth of east or west direction as long as mutual trough shading occurs. Therefore, this physical model is to a minor extent conservative.

A case structure differs between mutual trough shading in the morning and in the evening, as the SCAs affected are positioned in the west and in the east, respectively.

4 IMPLEMENTED CONTROL LOGICS

This chapter describes control logics introduced to the simulator during my engagement at DLR. First, chapter 4.1 quotes the tasks implemented to introduce the SGS control panel. Chapter 4.2 then deals with pressure control to prevent underinflation in the SGS return pipe. The automatic SF operation modes, which are currently available in the simulator (SF start-up mode and SF normal operation mode), are explained in chapters 4.3 and 4.4. Finally, protective control logics are outlined in chapters 4.5 and 4.6.

4.1 CONTROL PANEL FOR THE STEAM GENERATOR CYCLE

As described in chapter 2.2.2 there were two control elements concerning the steam generator cycle available at the main panel. According to predesigns of the actual control system, the main panel shows indicators of the test facility. Control elements, however, are only available in separate control panels. Therefore, it was necessary to design a control panel for the steam generator and connected piping. The predesigns of this control panel already showed the layout of the piping, positions of valves, buttons, control elements and indicators. The development task was to introduce a VI, duplicate the layout for the front panel, allow communication to other VIs via the connector panel and adjust the window management to enable the navigation between all control panels.

The established VI for the Steam Generator Panel also hosts the programming code for the calculation of the mixing temperature of the SH feed, as described in 3.4.1, and the evaluation of the valve opening for the pressure control of the Benson steam generator.

Figure 21 shows the newly developed Steam Generator Panel. The functionality of the Benson steam generator pressure control valve will be described in the next chapter.

4.2 PRESSURE CONTROL STEAM GENERATOR

The steam generation is done by a once-through Benson steam generator. Because of the SGS layout, the pipe connection of the SGS return branch is at 12.8 m height. Moreover, the salt then flows into the CT, with a height of 5.9 m (see Table 2). This change in height would lead to vacuum conditions in the SGS return pipe due to gravitational force. The plant design includes a valve which increases, dependent on the mass flow, the hydraulic resistance of this branch to prevent underinflation. [15]

According to the open-loop control strategy for the SGS return valve [15], the pressure drop across the valve can be written as:

$$\Delta p = \zeta \cdot \frac{\rho \cdot v^2}{2} = \zeta \cdot \frac{\rho \cdot \dot{V}^2}{2 \cdot A^2} \,, \tag{4.1}$$

with

$$\zeta = \frac{d^4}{625.44 \cdot K_V^2}$$

and

$$K_V = \frac{c_V}{1.1561}$$

Here, ζ represents the pressure drop coefficient, A the cross-section, ρ the density of the fluid and v and $\dot{V}$ the fluid flow velocity and the fluid flow rate, respectively. The pressure drop coefficient is calculated using the flow coefficient in m^3/h or in $US\ gal/min$ represented by K_V or c_V, respectively. Additionally, the inner diameter of the pipe and nominal valve diameter d is here used in mm.

To prevent vacuum at the highest point of the SGS an absolute static pressure of 1.015 bar must be secured by the SGS return valve. Static pressure at the inlet of the control valve can be calculated with:

$$p_{inlet} = p_\infty + \rho \cdot g \cdot (H_{SGS} - H) \,, \tag{4.2}$$

where p_{inlet} is the static pressure at the valve inlet, p_∞ is the ambient pressure, H_{SGS} is the maximum height of the SGS and H is the height of the control valve.

The pressure at the outlet of the control valve p_{outlet} is defined by the height of the pipe outlet at the cold tank H_{Tank}:

$$p_{outlet} = p_\infty + \rho \cdot g \cdot (H_{Tank} - H) \,. \tag{4.3}$$

To prevent vacuum at H_{SGS}, pressure drop over the valve needs to be:

$$\Delta p = p_{inlet} - p_{outlet} = \rho \cdot g \cdot (H_{SGS} - H_{Tank}) \tag{4.4}$$

Combining the pressure drop equations (4.1) and (4.4) results in:

$$\rho \cdot g \cdot (H_{SGS} - H_{Tank}) = \frac{1.1561^2}{625.4} \cdot \frac{d^4}{c_V^2} \cdot \frac{1}{2 \cdot A^2} \cdot \rho \cdot \dot{V}^2 \,. \tag{4.5}$$

The stroke s and the flow coefficient c_V are approximately related in a linear way and

$$c_V = c_{V,rel}(s) \cdot c_{Vs} \,, \tag{4.6}$$

where c_{Vs} describes the flow coefficient with the valve being totally opened and $c_{V,rel}(s)$ is the percentage of flow coefficient at the stroke opening s.

Introducing equation (4.6) into equation (4.5) and separating $c_{V,rel}(s)$ gives:

$$c_{V,rel}(s) = \sqrt{\frac{1}{g \cdot (H_{SGS} - H_{Tank})} \cdot \frac{1.1561^2}{625.4} \cdot \frac{d^4}{c_{Vs}^2} \cdot \frac{1}{2 \cdot A^2}} \cdot \dot{V}_{SGS} \tag{4.7}$$

The expression below the root function is a constant value defined by parameters of plant heights, the control valve and piping. The unit of the root function is s/m^3, so the volume flow $\dot{V}_{SGS}$ must be introduced in m^3/s.

Table 2: Parameter for the open-loop control of the SGS return valve

Symbol	Parameter	Value	Units
g	Gravity	9.81	m/s
H_{SGS}	Max. height of SGS	12.8	m
H_{Tank}	Height of return line to cold tank	5.91	m
d	Nominal inner pipe diameter	52.48	mm
A	Pipe cross-section	2.163e-3	m²
c_{Vs}	Flow coefficient	11.6	US gal/min

4.3 START-UP MODE OF THE SOLAR FIELD

The solar field start-up mode is one of the automatic operation modes which shall allow a reliable start-up of the SF without taking risks of dangerous plant states. As described in chapter 2.1.4, it is usually entered after sunrise or if sufficient irradiation is available. However, as the EMSP is a test facility it must be reliable and must prevent dangerous plant parameter at any time and independent of the point of activation.

The aim of this mode is to reach the SF nominal outlet temperature and therefore the SF normal operation mode as fast as possible without introducing impermissible temperature gradients. The idea is, that the earlier the nominal outlet temperature is reached, the more MS with a temperature as high as the nominal SGS temperature can be stored in the HT and therefore the more thermal energy can be used for electricity generation. On the other hand, the thermal energy generated in the SF before reaching the nominal outlet temperature is not lost completely but stored in the CT. There it increases the CT salt temperature and is, at best, recirculated into the SF or serves for the anti-freeze mode, as described in chapter 2.1.3. It cannot be denied, that operational strategies as well offer a wide range of research topics.

The challenge of the SF start-up mode is to restrict the temperature gradients of the receiver pipes to prevent thermal stresses and possible bending. Temperature gradients of 5 Kelvin per minute are the target value but should not be exceeded during start-up. Considering that, it was agreed on a step sequence to check multiple parameter to ensure a safe and reliable automatic start-up of the SF. [15]

4.3.1 IMPLEMENTED STEP SEQUENCE

The step sequence implemented to the simulator and described in this chapter describes the order as defined in [15].

Step 1: Checking preconditions

Pressing the Start-Up SF button activates the first step, where preconditions for this mode are checked. The second step is entered immediately if all these preconditions are fulfilled, otherwise a warning appears, and the start-up mode is deactivated again.

The preconditions are:

- CT pump 1 or 2 activated
- Cold header mass flow rate $> 1.3 \frac{kg}{s}$
- Cold header valve status > 75 %
- SF drainage valve status $= 0$ %
- HT inlet valve status $= 0$ %
- Bypass HT valve status > 75 %

Step 2: Establish maximum flow through the SF

The second step gives the command to establish the maximum mass flow through the SF to prevent freezing of the HTF on the one hand, and excessive temperature gradients and overheating of the HTF on the other hand. Therefore, the highest setpoint is given to the pump. If the mass flow rate exceeds a certain threshold, the step is completed.

Step 3: Focus all SCAs

The command to drive all SCAs into focus, results in a steep incline of temperature gradients if all the irradiation present hits the SCAs within seconds. Step 2 is therefore a preventive action to keep the temperature gradients as low as possible during this step.

Additionally, this step determines if there is enough effective irradiation available to heat the MS. While the mass flow rate remains at its maximum, the SF outlet temperature must rise 20 Kelvin higher than the SF inlet temperature to complete this step.

Step 4: Temperature gradient control

Since the SCAs are all driven into focus and the effective irradiation is sufficient to heat the MS, the goal is to reach the nominal outlet temperature with a constant temperature gradient. A maximum temperature gradient of 5 Kelvin per minute is required. A PID controller is implemented to adjust the operating point of the CT pump if the measured maximum temperature gradient differs from the setpoint. The temperature gradients of each SCA are averaged over the last 30 seconds and extrapolated to a temperature gradient per minute. The maximum value of all four temperature gradients acts as the measured process variable for the PID controller. The temperature gradient control remains activated until the end of the SF start-up phase. The next step is entered if the SF outlet temperature reaches 390 °C.

Step 5: Redirect MS mass flow into the HT

Step 5 gives the command to completely open the HT inlet valve and close the bypass HT valve. The MS is no longer recirculated into the CT but added to the HT. Reaching an SF outlet temperature of 500 °C concludes this step.

Step 6: Activate SF normal operation mode

The SF normal operation mode is deactivated, and normal operation mode is entered.

4.4 NORMAL OPERATION MODE OF THE SOLAR FIELD

The SF normal operation mode implies that the receivers and pipes of the SF cycle are already warmed up and the outlet temperature of the SF is approximately the nominal outlet temperature. The aim of this automatic operation mode is to control the mass flow rate if the SF outlet temperature differs from the nominal outlet temperature. Using the automatic mass flow controller is set as a default when operation mode switches from start-up to normal operation. However, the operator can also choose to set a mass flow rate manually. [15]

The mass flow controller of the automatic normal operation mode is a feed-forward control. The operating point of the CT pump is evaluated depending on the setpoint of the SF outlet temperature $\vartheta_{out,set}$, the effective irradiation g_{Eff} and a scale factor. The scale factor f_{scale} allows considering factors like mirror soiling and can be adjusted by the operator. It was decided to use a feed-forward control to allow a fast response to changes in DNI. More complex simulation tools would use control strategies where feed-forward and feed-back controllers are combined. [19]

The mass flow setpoint of the normal operation mode is calculated as:

$$\dot{m}_{set} = f_{scale} \cdot \frac{\eta \cdot g_{Eff} \cdot A_a}{c_p \cdot \left(\vartheta_{out,set} - \vartheta_{in}\right)}\,, \tag{4.8}$$

where η is an assumption of the SF optical and thermal efficiency ($\sim$65%). Furthermore, $g_{Eff} \cdot A_a$ gives the effective irradiation on the SF aperture area A_a and the term $c_p \cdot \left(\vartheta_{out,set} - \vartheta_{in}\right)$ describes the enthalpy difference of the MS over the loop at nominal outlet temperature.

During manual control, a PID feed-back controller is used to adjust the operating point of the CT pump, to reach the mass flow rate setpoint entered by the operator.

4.5 TRACK RELEASE SIGNAL

The track release signal is a control logic to protect the SF from inadmissible operation states. It is a Boolean signal. The track release signal being “False”, disables driving any SCA into or through the focus. A track release signal which is “True” allows to give the “Track” command and therefore to drive the SCAs into focus. Consequently, if the

SCAs are focused to the sun and the track release signal switches from “True” to “False”, the SCAs are forced into “Defocus” mode, meaning that they are following the movement of the sun with a delay of 2.3°, preventing energy input to the receiver tubes. Details on the operation modes of the SCAs are given in [12].

According to the functional description [15] all criteria mentioned must be met for track release $= "True"$:

- CT pump 1 or 2 activated
- Cold header mass flow rate $> 1.3 \frac{kg}{s}$
- Cold header mass flow measurement channel fault $= "False"$

The mass flow measurement channel fault would indicate a failure of the mass flow measurement device but is not yet implemented to the simulator.

4.6 PROTECTIVE TANK LEVEL LIMIT CONTROL

As mentioned in chapter 2.1.3, upper and lower level limits, which must not be exceeded, are defined for all salt tanks of the EMSP. The level limits should mainly prevent overfilling of the tanks and protect the pumps from operation at low salt levels which could lead to dry running.

4.6.1 STORAGE TANKS

The storage tanks are cylindrical tanks with a diameter of 3.1 metres and a height of 5 metres. The lower level limit is at a height of 0.6 metres to prevent the CT pumps and the HT pumps from dry running. If this height is reached, the control system automatically gives the command to turn off the pumps of the regarding tank. The upper level limit is at 4.4 metres and results in an automatic closure of all inlet valves. [12] [15]

4.6.2 DRAINAGE TANK

The drainage tank is, as described in 3.2, a horizontal cylindrical tank with a diameter of 1.8 metres and a cylinder height of 5.1 metres. The lower level limit of this tank is at 0.4 metres and leads to an automatic shutdown of the DP if it is reached. When reaching the upper level limit of 1.0 metres, all pumps (HT and CT pumps) are deactivated to prevent further salt flow into the tank. [12] [15]

5 RESULTS AND DISCUSSION

Great value was set upon bug-fixing and keeping the code as comprehensible as possible, while improving the EMSP simulator. The following subchapter will briefly discuss the HMI of the simulator. Screenshots can be seen in the Appendix in chapter 9. Some of the physical models and control logics implemented, as described in chapter 3 and chapter 4, will be outlined on the basis of a showcase simulation in 5.2.

5.1 SIMULATOR HUMAN MACHINE INTERFACE

The layout of the simulator HMI is similar to predesigns of the actual control system. Exemplarily, Figure 10 shows a first draft of the Cold Salt Tank panel, while the layout of the regarding simulator panel can be seen in Figure 11.

The main panel of the simulator shows indicators of the test facility and gives an impression over the state of the plant. Furthermore, it allows the navigation to all control panels and provides the options to start, pause, restart or end the simulation, save the simulation data, display the simulation live chart or a table of data history. According to chapter 2.2.4, all component control elements which were previously available at the main panel were transferred to the newly developed Steam Generator Panel, which can be seen in Figure 21. The buttons to enter the SF automatic operation modes were introduced to the main panel and can be seen in Figure 17. [26]

Obviously, commercial control systems would not only provide a main panel and various control panels, but several component panels indicating, for example, vibrations of the pumps or the like. However, the current design of the simulator HMI is entirely satisfactory, as the main purpose of the simulator is the operator training, which should allow to get acquainted with the behaviour of the EMSP salt cycle. All panels and windows of the simulator can be seen in the Appendix in chapter 9.

Starting the EMSP simulator a window appears where the simulator mode needs to be chosen (Figure 15). The test mode was established for software development purposes only. Entering the operation mode, opens the simulation initialization window as shown in Figure 16. The operator can choose between a set of starting and boundary conditions for the simulation and finally enters the control system by pressing the OK button.

The main panel, as displayed in Figure 17, acts as a starting point of the simulation and remains permanently opened. Navigation to the control panels and amongst the control panels is done via the dark grey square buttons.

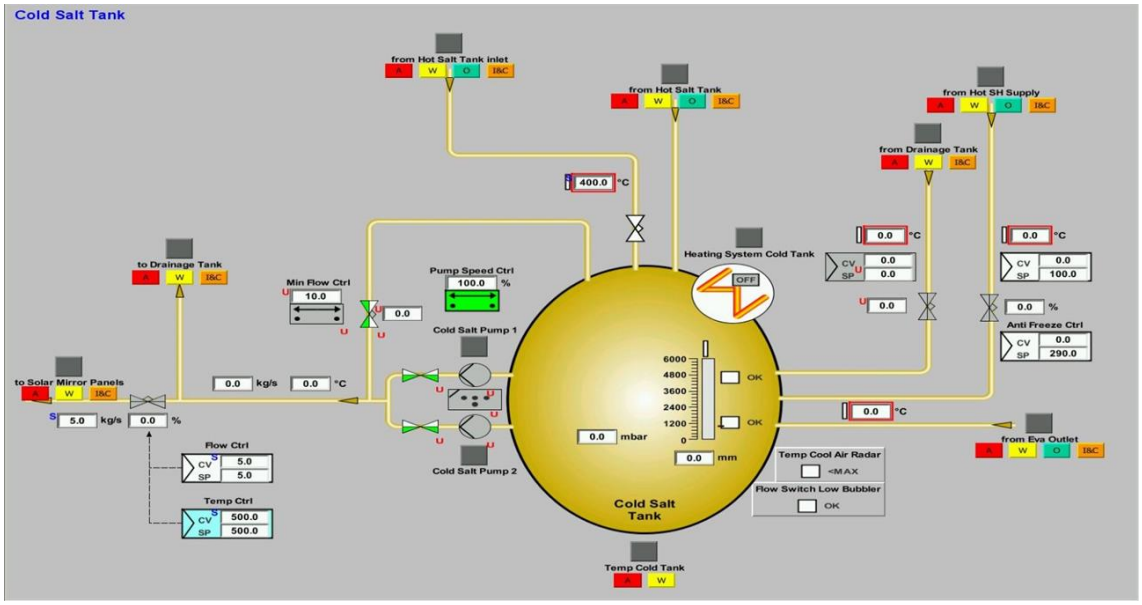

Figure 10: Predesign of the actual process control software (Cold Salt Tank panel) [26]

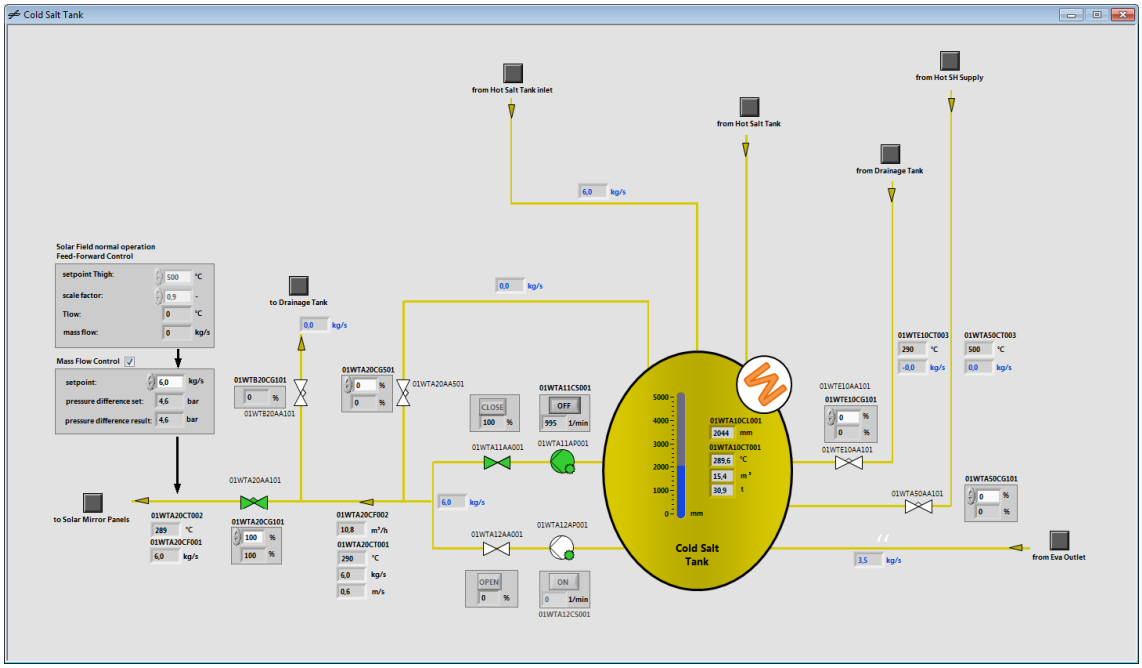

Figure 11: Design of the simulator HMI (Cold Salt Tank panel)

5.2 SHOWCASE SIMULATION

The showcase simulation is based on weather data of the PSA from 29 January 2013. The weather data represent a cloudy day and the starting time was set to 08:20 when sun rises to demonstrate the implemented automatic operation modes of the simulator. The chart, displayed in Figure 12, clearly shows the cloudy weather conditions during the time of simulation from 08:20 to 11:15. Additionally, the difference between the DNI and the effective irradiation g_{Eff} can be seen. To recur to the point described in 2.2.2, the effective irradiation as displayed in the live chart, data history or exported data of the simulator includes not only the IAM and end losses but also the modelled mutual trough shading as described in chapter 3.5. Therefore, SCA 3 and SCA 4 which are positioned further east are shadowing SCA 1 and SCA 2 in the morning. Mutual trough shading ends at 10 o`clock as the sun reaches a zenith angle of 69°.

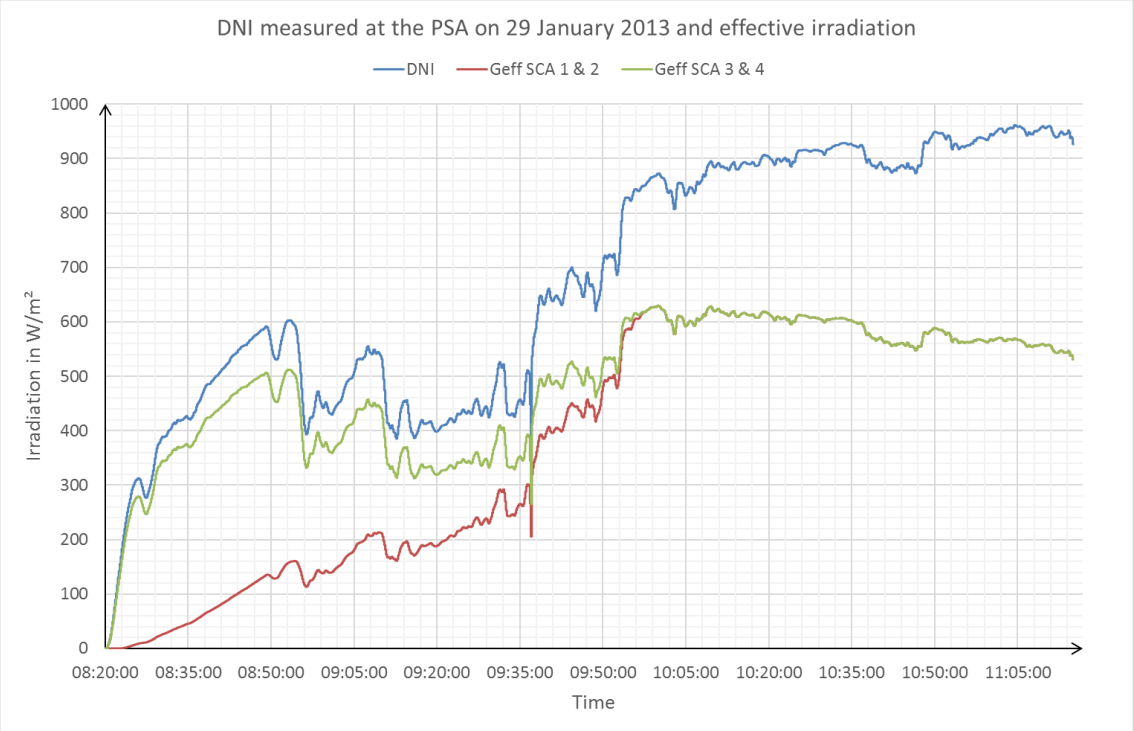

Figure 12: Showcase simulation - Chart of DNI and effective irradiation

Except the day and the time, all data of the simulation initialization remained at the default values as shown in Figure 16.

5.2.1 Simulation Results – Solar Field Start-Up

The simulation was started at 08:20 and the automatic SF start-up mode was entered at 08:22 with an effective irradiation of about 90 W per square meter. Figure 13 displays the most important parameters during the SF start-up sequence. Tout_SF shows the SF outlet temperature, m_dot_SF indicates the mass flow and T_grad_max displays the maximum temperature gradient which, as described in chapter 4.3, should not exceed 5 Kelvin per minute to prevent thermal stresses and possible bending of the SCA receiver pipes.

The start-up mode was entered at ① and, according to 4.3.1, the preconditions were checked, and the mass flow rate ramped up to the maximum flow rate. As the mass flow through the SF increased, a threshold was exceeded, indicating that the maximum flow rate was reached. As described in 4.3.1, Step 3 was entered and the SCAs were driven into focus. This can be seen in Figure 13, as the maximum temperature gradient is increasing shortly after point ①. The maximum mass flow rate prevented excessive temperature gradients and remained active until ②.

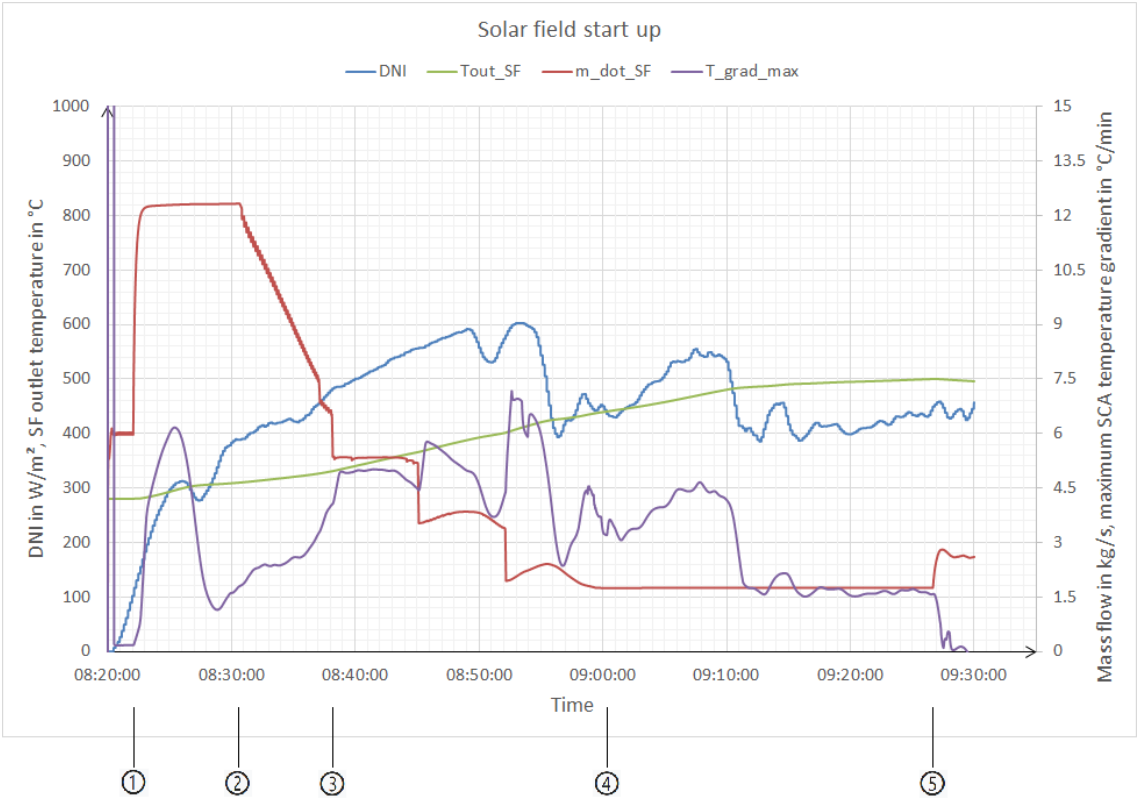

Figure 13: Showcase simulation - Chart of parameters during SF start-up

At ② the SF outlet temperature reaches 310 °C or better to say, 20 Kelvin more than the SF inlet temperature, indicating that the irradiation was sufficient to heat up the MS and operate the SF in normal operation. Consequently, the temperature gradient control was activated to reach the normal operation mode as fast as possible while preventing excessive temperature gradients. As displayed in Figure 13 between ② and ③, the temperature gradient controller decreased the MS mass flow rate to increase the temperature gradient to the setpoint of 5 Kelvin per minute.

A steep decline of mass flow rate can be examined shortly before, and at ③, as well as twice between ③ and ④. The reason was an intervention of the operator due to low rotational speed of the cold pump. The lower limit of the CT pump rotational speed is at 850 rpm. As the temperature gradient controller adjusted the operating point of the pump to decrease the mass flow rate, the rotational speed approached this lower limit. The operator therefore decremented the cold header valve opening by 20% to allow even lower mass flow rates and maintain the temperature gradients. However, the temperature gradients again dropped below the setpoint because of the rotational speed limit. At 08:52 the cold header valve opening was set to 20% and remained at this point. At ④ the CT pump again reached the lower limit of the rotational speed, resulting in a mass flow rate of 1.7 kg/s. According to 4.5 Track Release Signal, a mass flow rate smaller than 1.3 kg/s would force the SCAs into "Defocus" mode. Hence, the operator decided to keep the setting of the cold header valve opening at 20%.

At ⑤ the SF outlet temperature reached 500 °C and the automatic operation mode switched to the SF normal operation.

Conclusively, the SF start-up sequence of this showcase simulation shows the importance of operator expertise. Cloudy conditions can lead to both, steeply decreasing and increasing temperature gradients during SF start-up. Further developments would include controller tuning to speed up the controller response and the implementation of a controller for the cold header valve. Such a controller, however, is not yet defined in the functional description of the HPS2 project and therefore not available in the simulator, for the training of the operator staff.

5.2.2 Simulation Results – Solar Field Normal Operation Mode

Figure 14 displays the most important parameters during the automatic SF normal operation mode. The SF start-up mode was deactivated, and the SF normal operation mode was entered automatically at 09:27 when the outlet temperature first reached 500 °C. Switching the operation mode also changes the mass flow control. The aim of this mode is not to achieve a temperature increase of 5 Kelvin per minute as during the SF start-up mode, but to maintain the SF outlet temperature. Therefore, entering the normal operation mode results in a sudden increase of mass flow rate, as can be seen in Figure 14. The mass flow feed-forward control of this automatic operation mode, as described in chapter 4.4, evaluates the operation point of the CT pump depending on the setpoint of the SF outlet temperature, the effective irradiation and the scale factor. During the showcase simulation, the setpoint of the SF outlet temperature remained at the default value of 500 °C. Similar to the situation described in 5.2.1, the operator this time incremented the cold header valve opening to 40% shortly before 09:40 to avoid reaching the maximum rotational speed limit of the CT pump. Furthermore, small adjustments to the scale factor were necessary until 10:00 to keep the outlet temperature close to 500°C.

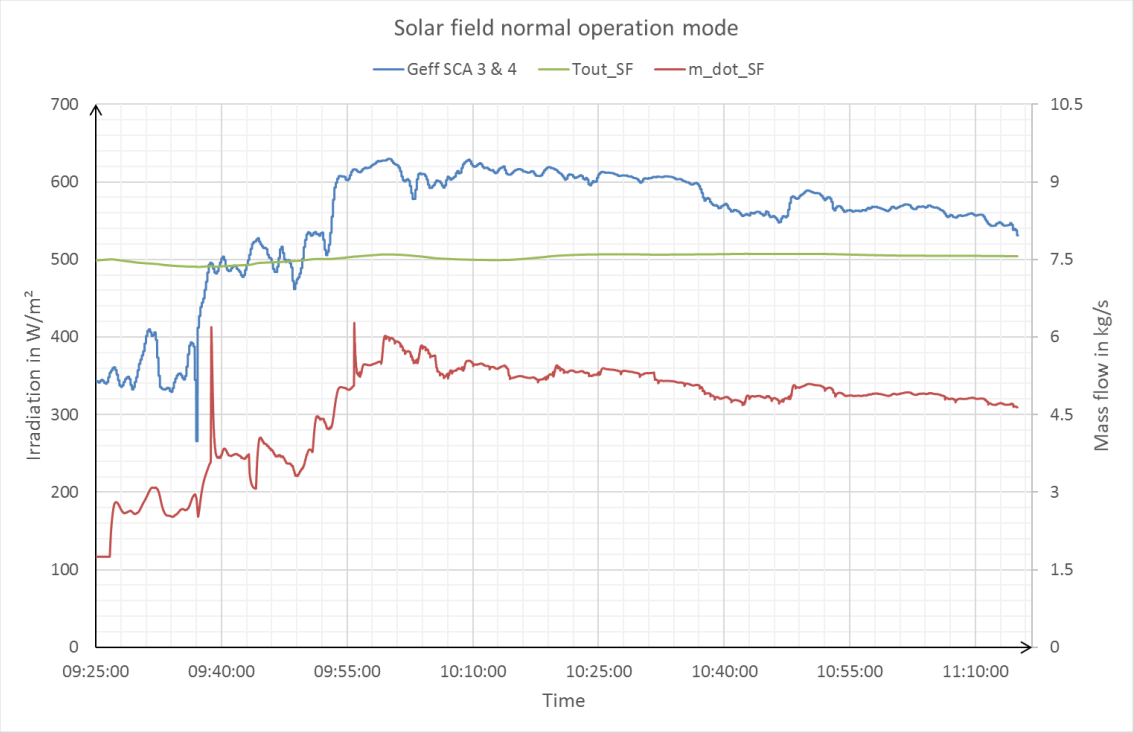

Figure 14: Showcase simulation - Chart of parameters during SF normal operation

The adjustments to the scale factor can be identified in Figure 14, as the mass flow rate nearly exactly follows the shape of the effective irradiation if no parameters of the feed-forward control are changed. The problems of the feed-forward control are obvious. As described in 4.4, the SF optical and thermal efficiency is assumed to be 65%, however, this parameter of converting solar irradiation to thermal energy cannot be constant while the boundary conditions or ambient conditions vary over time. Furthermore, as shown in Figure 12, SCA 1 and SCA 2 are still affected by mutual trough shading until 10:00. The feed-forward control, however, uses the maximum effective irradiation to evaluate the mass flow rate. Using a weighted average effective irradiation could improve the behaviour during mutual trough shading. Conclusively, the actual control system will use more complex control strategies, with a possible combination of feed-forward and feed-back control to improve the behaviour during SF normal operation mode. The feed-forward control is a solution which introduces the scale factor to the operators and shows good behaviour. Further developments or possible follow-up projects could deal with controller tuning or advanced control strategies.

6 CONCLUSION AND OUTLOOK

The main goal of all further developments and implementations to the EMSP simulator was to characterise the salt cycle as accurate as possible with reasonable effort and to establish all automatic operation modes for the solar field, so that a simulation over one day without manual control would be possible (assuming fair ambient conditions).

Therefore, the salt cycle of the simulator was completed, by introducing components which were not modelled prior to this thesis, like various valves or the drainage tank and equipment. A model for mutual trough shading was implemented, which results in a higher simulation accuracy during solar field start-up. Mass flow distribution within pipework is modelled considering hydraulic resistances of pipes, bends and valves, as well as the pressure drop across the steam generator.

Furthermore, control logics for different operation modes of the solar field or protective control logics, like level limits for all tanks or the track release signal for the solar field operation, were implemented. The automatic solar field operation modes do not involve the normal or fast shut-down sequences or the convective anti-freeze mode, as defined in the functional description, yet.

Finally, the human machine interface of the simulator was finalised according to pre-designs of the actual control system. In its current stage, the simulator will allow to show the basic structure of the actual control system and demonstrate the basic behaviour of the molten salt system.

It will be used to provide foregoing training to the staff with no risk of damage to the components. Participating operators can provide feedback before commissioning of the research test plan and therefore potentially increase the operability of the test facility. Different control strategies could be tested before commissioning or during operation to optimize the output of the molten salt parabolic trough test facility.

7 LIST OF ABBREVIATIONS

Abbreviation	Explanation
CDI	Cold Distributor Inlet
CDO	Cold Distributor Outlet
CP	Cold Tank Pump
CSH	Cold Superheater Supply
CSP	Concentrating Solar Power
CT	Cold Tank
DLR	Deutsches Zentrum für Luft- und Raumfahrt e. V. (German Aerospace Center)
DNI	Direct Normal Irradiation
DP	Drainage Tank Pump
DT	Drainage Tank
ECO	Economiser
EMSP	Évora Molten Salt Platform
EVA	Evaporator
EVAout	Evaporator outlet
HDI	Hot Distributor Inlet
HDO	Hot Distributor Outlet
HMI	Human Machine Interface
HP	Hot Tank Pump
HPS2	High Performance Solar 2
HSH	Hot Superheater Supply
HT	Hot Tank
HTF	Heat Transfer Fluid
IAM	Incidence Angle Modifier
LCoE	Levelized Costs of Electricity
MS	Molten Salt
PSA	Plataforma Solar de Almería
SCA	Solar Collector Assembly
SEGS	Solar Electric Generation Stations (parabolic trough power plants in the Mojave Desert of California)
SF	Solar Field
SGS	Steam Generation (Generator) System
SH	Superheater

SHFeed	Superheater Feed
TES	Thermal Energy Storage
VI	Virtual Instrument
VSF	Virtual Solar Field

8 REFERENCES/BIBLIOGRAPHY

[1] DLR Institute of Solar Research, "Home," [Online]. Available: https://www.dlr.de/sf/en/. [Accessed 31 July 2018].

[2] S. A. Kalogirou, Solar Energy Engineering: processes and systems, Elsevier Inc., 2009.

[3] D. Y. Goswami, F. Kreith and J. F. Kreider, Principles of Solar Engineering, 2nd ed., Taylor & Francis, 1999.

[4] DLR Institute of Solar Research, "Research and Development > Line Focus Systems > Molten Salt Systems," [Online]. Available: http://www.dlr.de/sf/en/desktopdefault.aspx/tabid-10647/18795_read-44147/. [Accessed 26 June 2018].

[5] DLR Institute of Solar Research, "News > News Archive > Molten salt instead of thermal oil in solar thermal parabolic trough plants shall reduce the levelized electricity costs," 15 December 2016. [Online]. Available: http://www.dlr.de/sf/en/desktopdefault.aspx/tabid-10436/20174_read-48143/. [Accessed 27 June 2018].

[6] D. Kearney, U. Herrmann, P. Nava, B. Kelly, R. Mahoney, J. Pacheco, R. Cable, N. Potrovitza, D. Blake and H. Price, "Assessment of a Molten Salt Heat Transfer Fluid in a Parabolic Trough Solar Field," *Journal of Solar Energy Engineering*, vol. 125, pp. 170-176, May 2003.

[7] DLR Institute of Solar Research, "Research and Development > Point Focus Systems > Solarthermal Receivers," [Online]. Available: http://www.dlr.de/sf/en/desktopdefault.aspx/tabid-10645/18495_read-43274/. [Accessed 27 June 2018].

[8] M. Wittmann and K. Hennecke, "HPS2 – High Performance Solar 2: Évora Molten Salts Platform," *Presentation,* [Online]. Available: https://elib.dlr.de/108981/. [Accessed 26 July 2018].

[9] H. Silva, "HPS2 - High Performance Solar 2," [Online]. Available: http://www.emsp.uevora.pt/. [Accessed 27 June 2018].

[10] M. Wittmann, M. Schmitz, H. G. Silva, P. Schmidt, G. Doppelbauer, R. Ernst, P. Santamaria and T. Miltkau, "HPS2 – Demonstration of Molten-Salt in Parabolic Trough plants," *Abstract, SolarPACES 2018, Internal documentation,* 2018.

[11] TSK Flagsol, "Collector Properties - Basic Engineering," *Internal documentation,* 1 March 2018.

[12] T. Hirsch, "Entwicklung eines Trainingssimulators für den Solarfeld- und Speicherbetrieb eines solarthermischen Parabolrinnenkraftwerkes," *Bachelor thesis,* [Online]. Available: https://elib.dlr.de/113530/. [Accessed 26 June 2018].

[13] M. Wittmann, "The Évora Molten Salt Plattform - Anlagenkonzept und Testmöglichkeiten," *Presentation, DLR-Sonnenkolloquium 2017, Cologne,* [Online]. Available: https://www.dlr.de/Portaldata/73/Resources/dokumente/soko/soko2017/praesentationen/DLR-Sonnenkolloquium2017_Evora_-_Michael_Wittmann_fin.pdf. [Accessed 26 June 2018].

[14] J. F. Feldhoff, T. Hirsch und T. Hirsch, „Training Simulator for Molten Salt Parabolic Trough Test Plant," *Poster, SolarPACES 2017, Santiago de Chile,* September 2017. [Online]. Available: https://elib.dlr.de/114703/. [Accessed 26 June 2018].

[15] DLR, „Functional Description Molten Salt Cycle," *Internal documentation,* 2017.

[16] B. Mütterlein, Handbuch für die Programmierung mit LabVIEW: mit Studentenversion LabVIEW 2009, 2. Hrsg., Spektrum Akademischer Verlag, 2009.

[17] DLR Institute of Solar Research, "Services > Simulations & Projections > Virtual Solar Field (VSF)," [Online]. Available: http://www.dlr.de/sf/en/desktopdefault.aspx/tabid-11690/20444_read-47787/. [Accessed 27 June 2018].

[18] K. Noureldin, T. Hirsch and R. Pitz-Paal, "Virtual Solar Field - Validation of a detailed transient simulation tool for line focus STE fields with single phase heat transfer fluid," *Solar Energy 146,* pp. 131-140, 1 March 2017. [Online]. Available: https://elib.dlr.de/111372/. [Accessed 26 June 2018].

[19] K. Noureldin, „Modelling and Optimization of Transient Processes in Parabolic Trough Power Plants with Single-Phase Heat Transfer Fluid," *(Unpublished Doctoral Dissertation); Mechanical Engineering Department, RWTH Aachen,* 2018.

[20] N. P. Siegel, R. W. Bradshaw, J. B. Cordaro and A. M. Kruizenga, "Thermophysical Property Measurement of Nitrate Salt Heat Transfer Fluids," in *Proceedings of the ASME 2011 5th International Conference on Energy Sustainability,* Washington, DC, 2011.

[21] M. Seitz and M. Krüger, "CSPBankability Project Report: Draft for an Appendix E - Thermal Energy Storage to the SolarPACES Guideline Bankable STE Yield Assessment," January 2017. [Online]. Available: https://www.dlr.de/sf/de/desktopdefault.aspx/tabid-11126/19467_read-48251/. [Accessed 05 August 2018].

[22] P. K. Swamee and A. K. Sharma, Design of Water Supply Pipe Networks, John Wiley & Sons, 2008.

[23] S. W. Churchill, „Friction-factor equation spans all fluid-flow regimes," University of Pennsylvania, 1977.

[24] F. M. White, Fluid Mechanics, 7. ed., McGraw Hill, 2011.

[25] J. Wang, J. Wang, X. Bi and X. Wang, "Performance Simulation Comparison for Parabolic Trough Solar Collectors in China," *International Journal of Photoenergy*, vol. 2016, [Online]. Available: https://www.hindawi.com/journals/ijp/2016/9260943/. [Accessed 26 June 2018].

[26] D. Hoegemann, K. Noureldin, F. Bamberger and T. Hirsch, "Development of Training Simulator Software for Molten Salt Parabolic Trough Test Platform," *(Unpublished Paper), SolarPACES 2018, Casablanca, Morocco,* August 2018.

9 APPENDIX

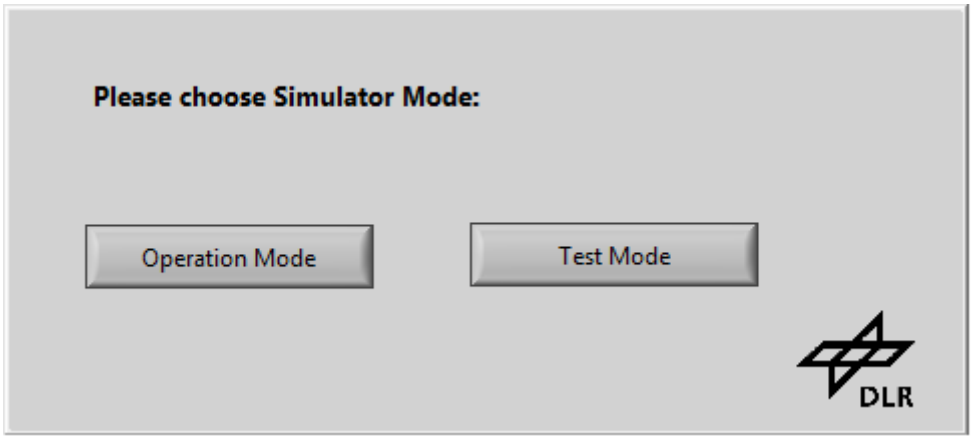

Figure 15: Choose simulation mode after starting the EMSP simulator

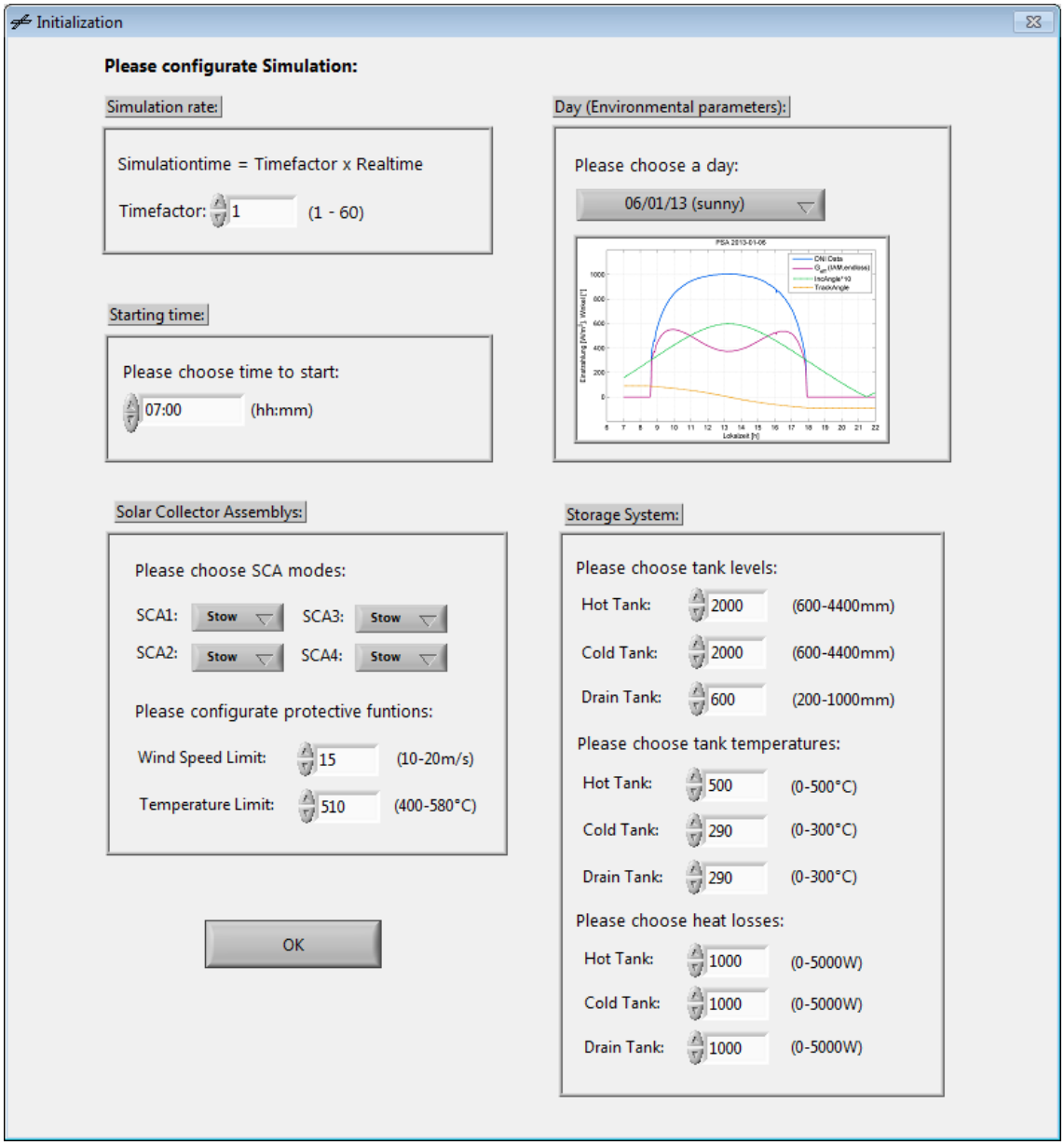

Figure 16: Initialization window of the operation mode

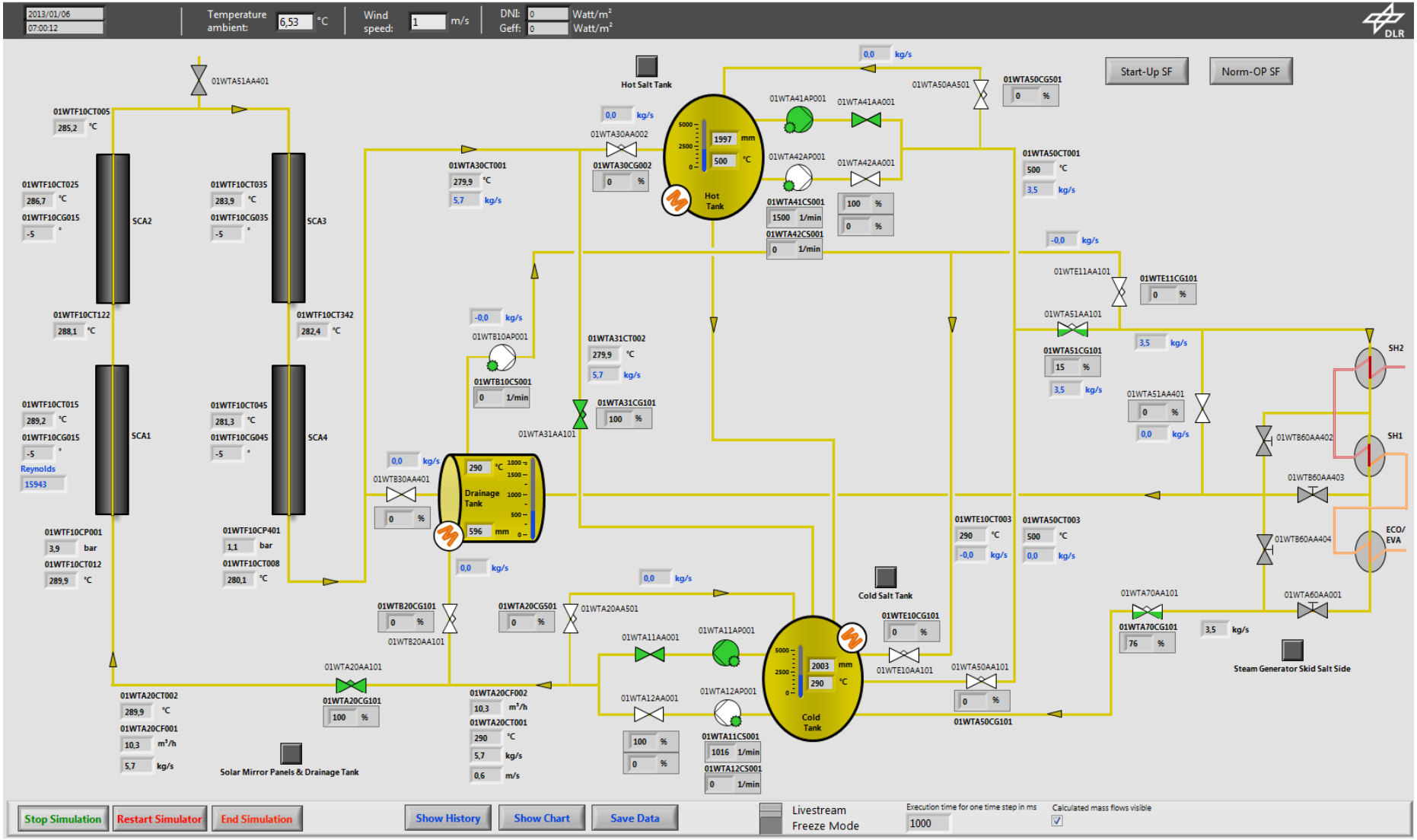

Figure 17: Main panel design

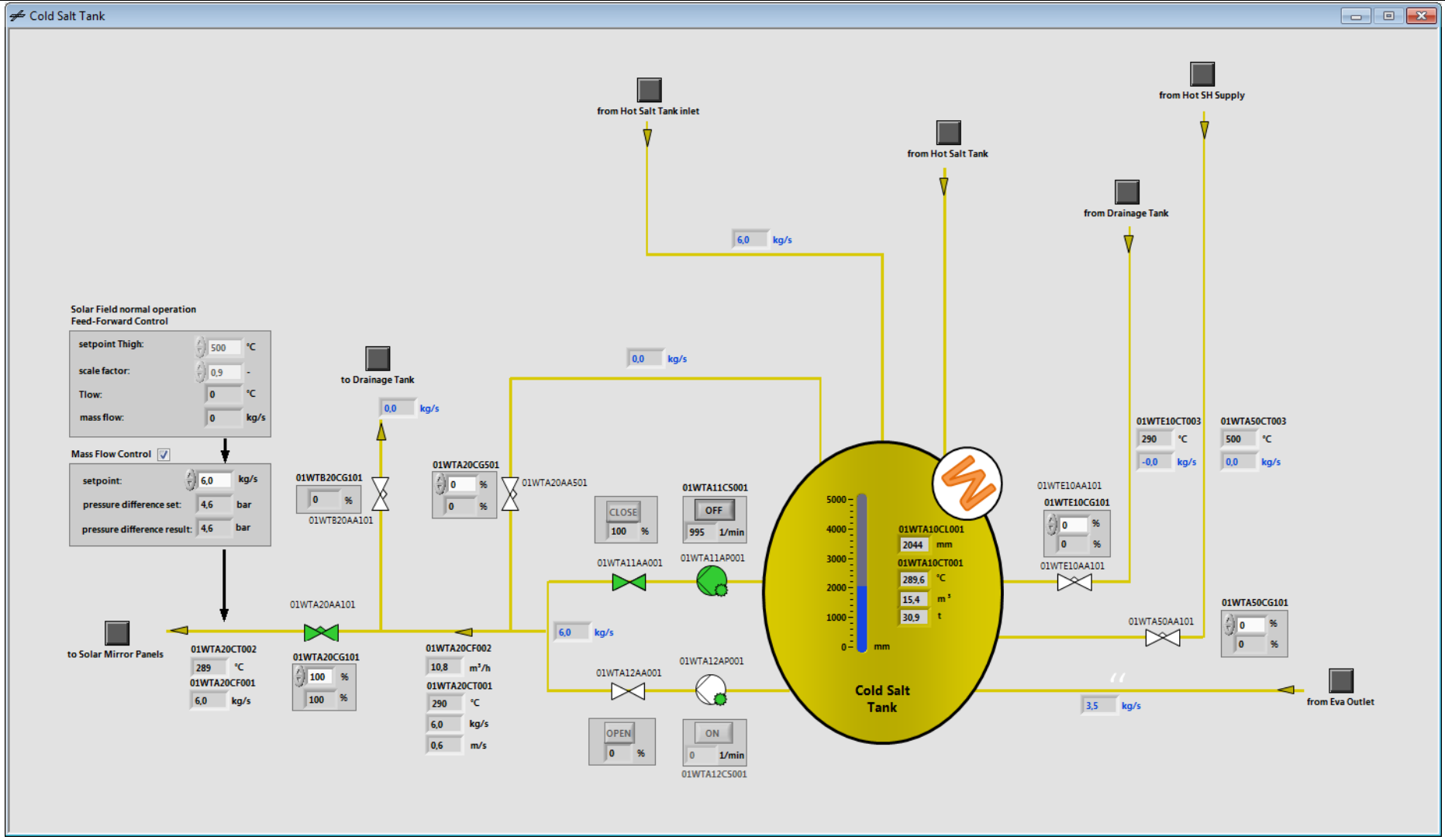

Figure 18: Cold salt tank control panel

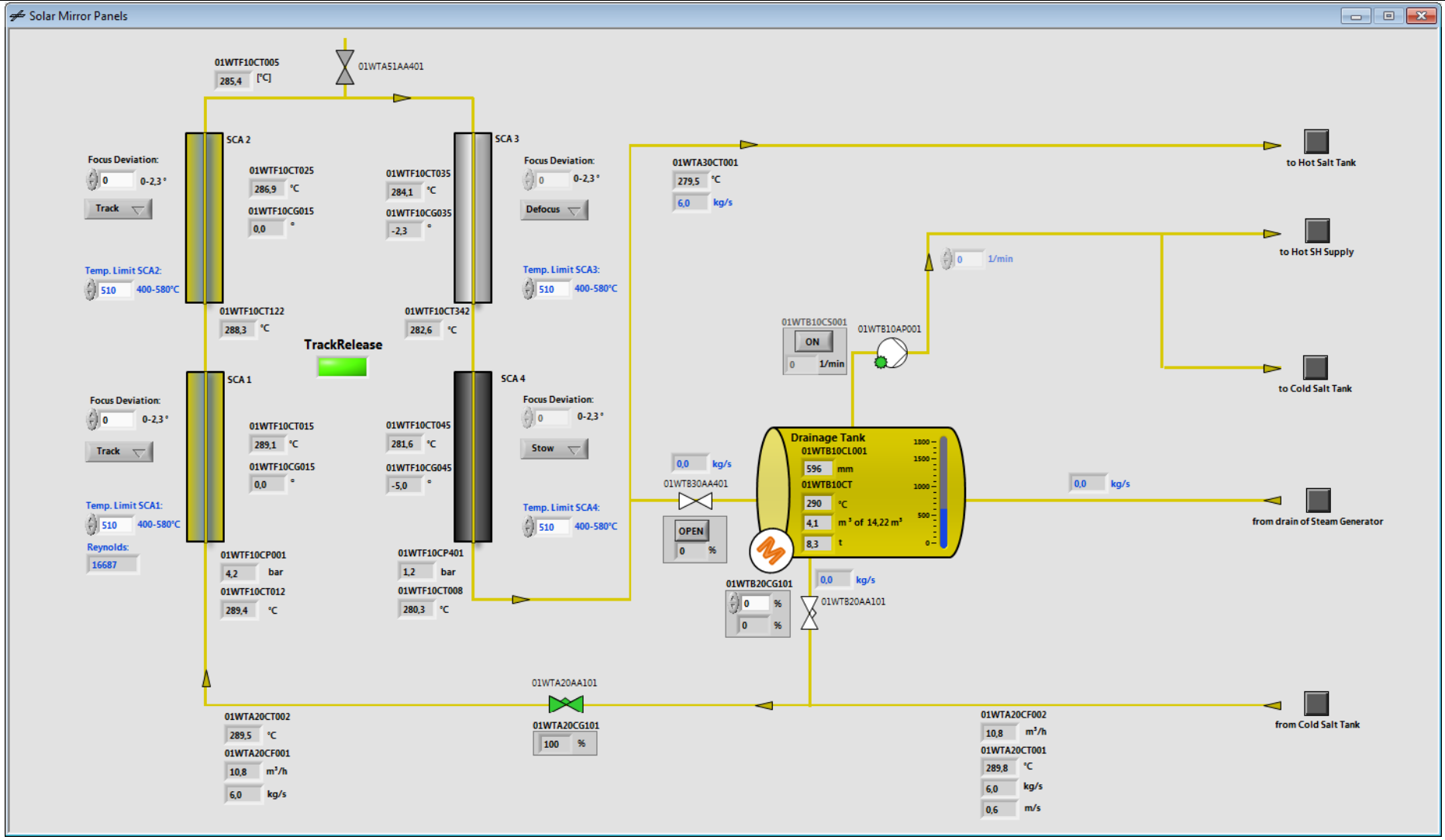

Figure 19: Solar mirrors and drainage tank control panel

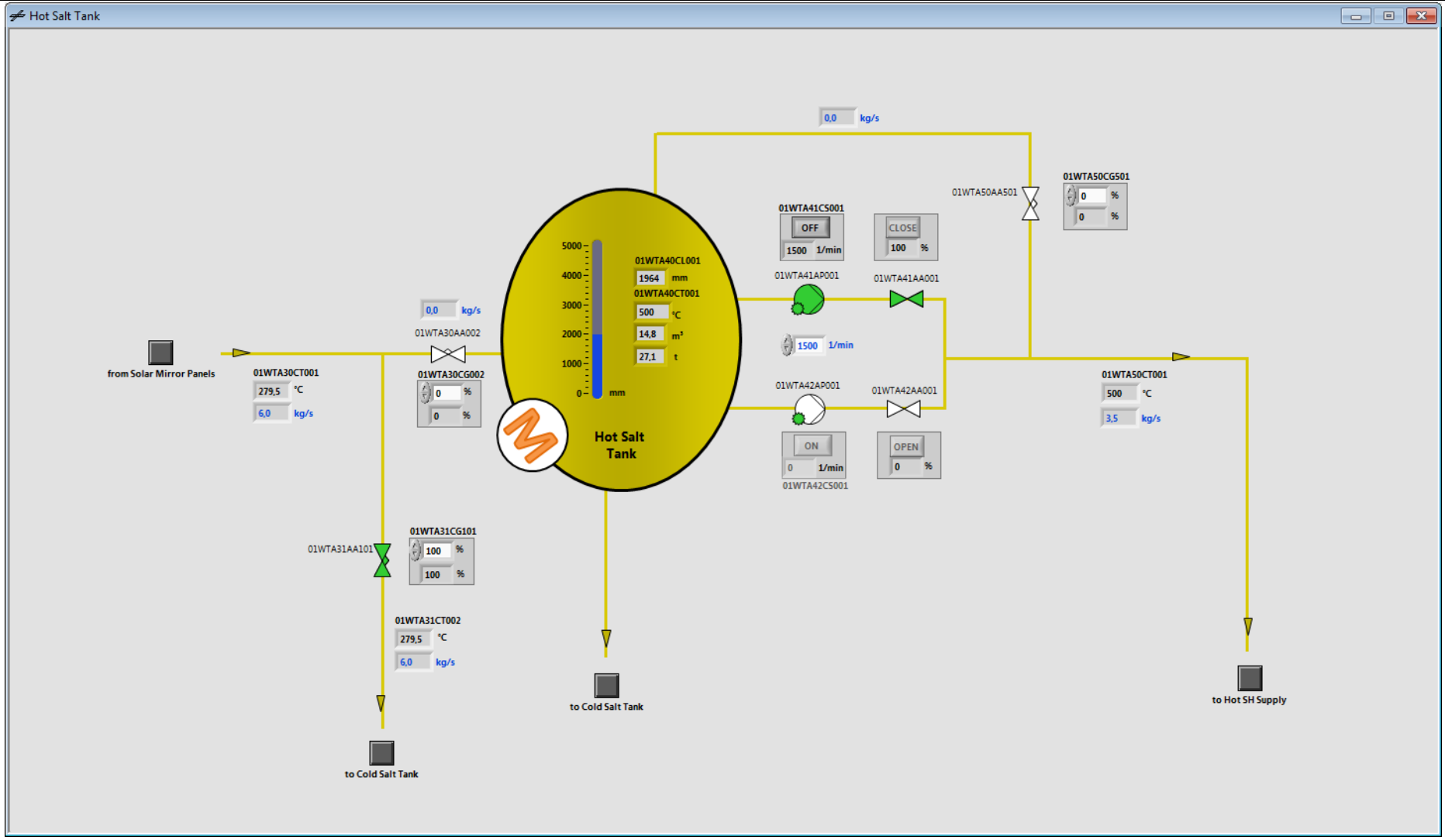

Figure 20: Hot salt tank control panel

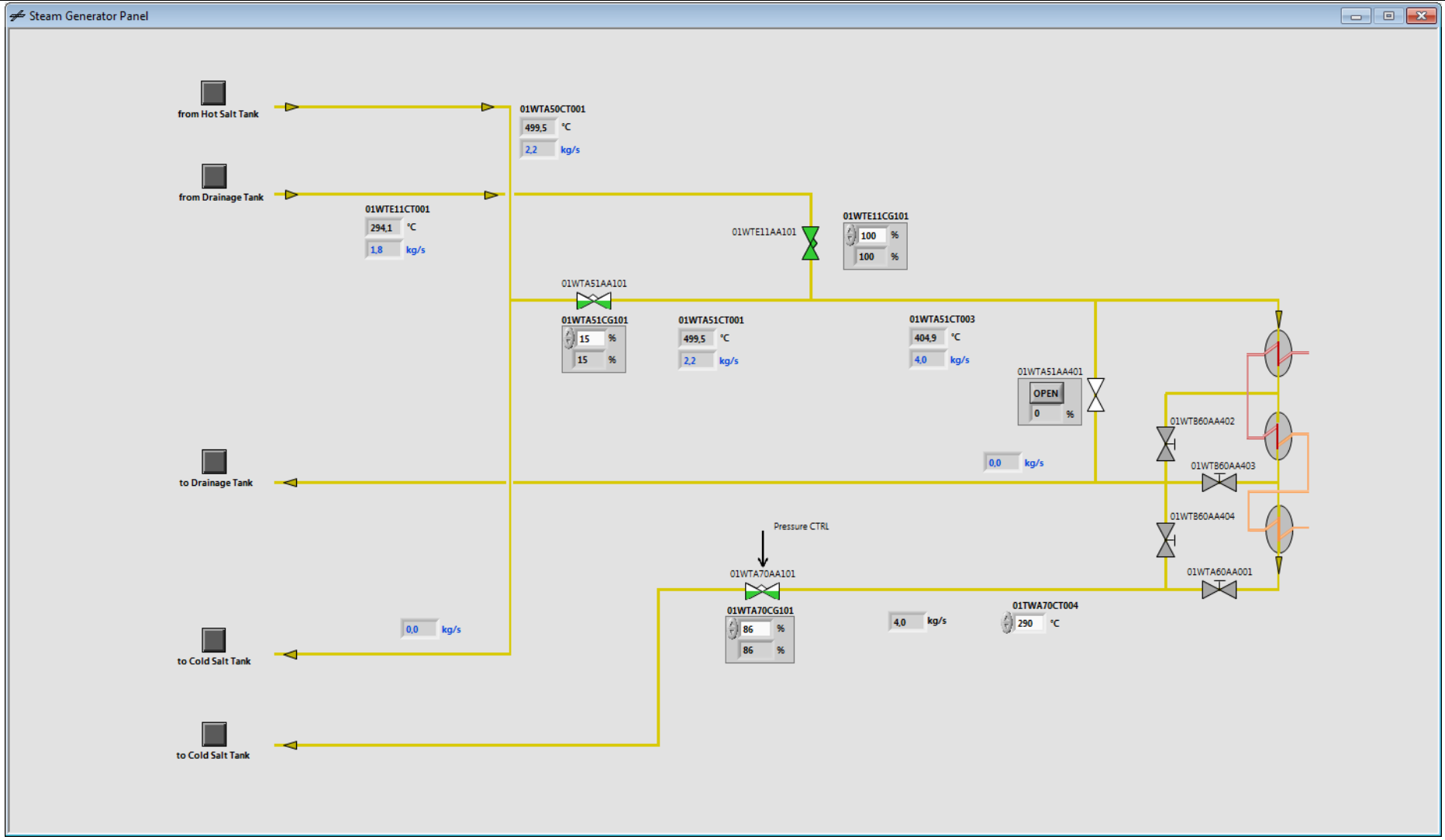

Figure 21: Steam generator control panel

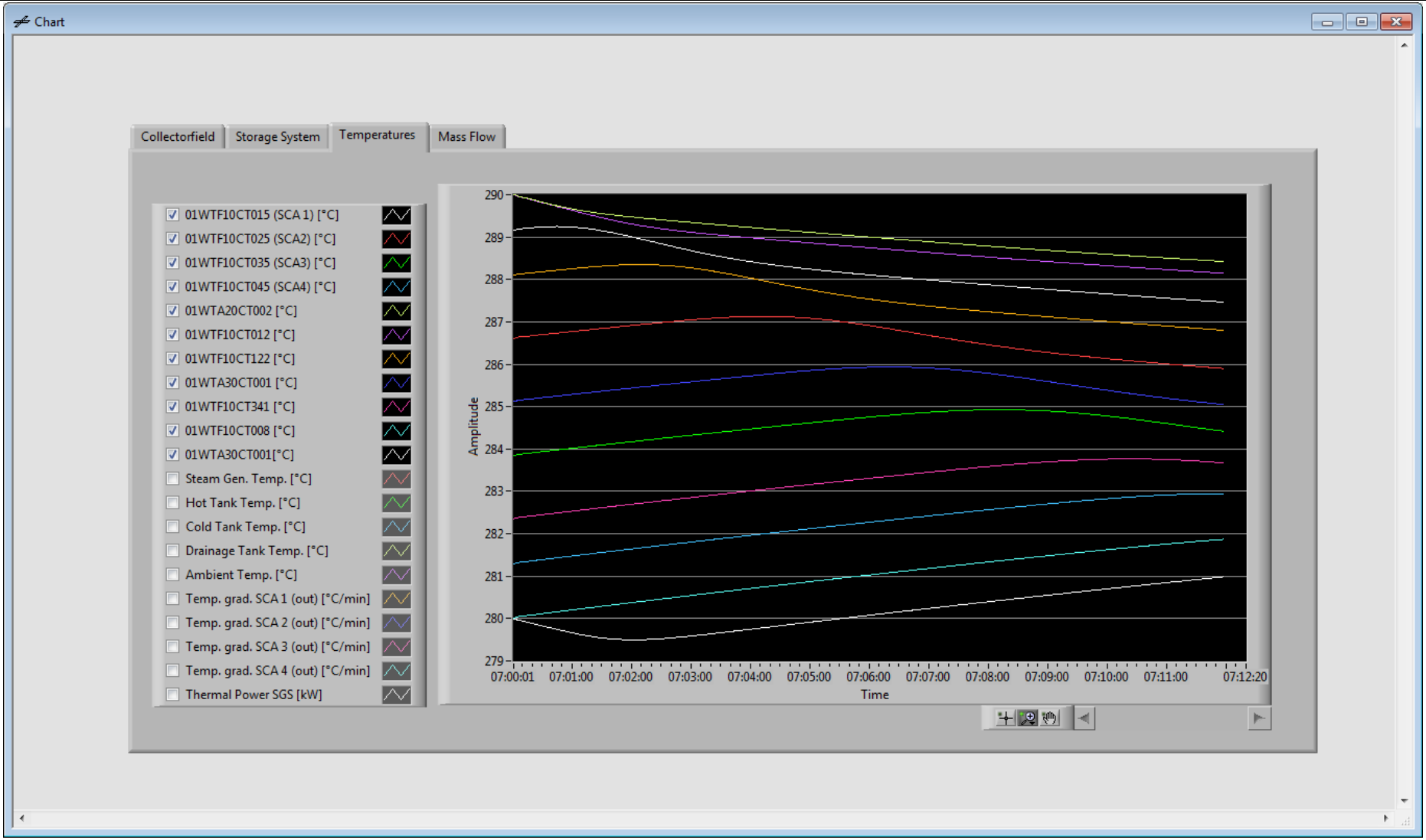

Figure 22: Chart window

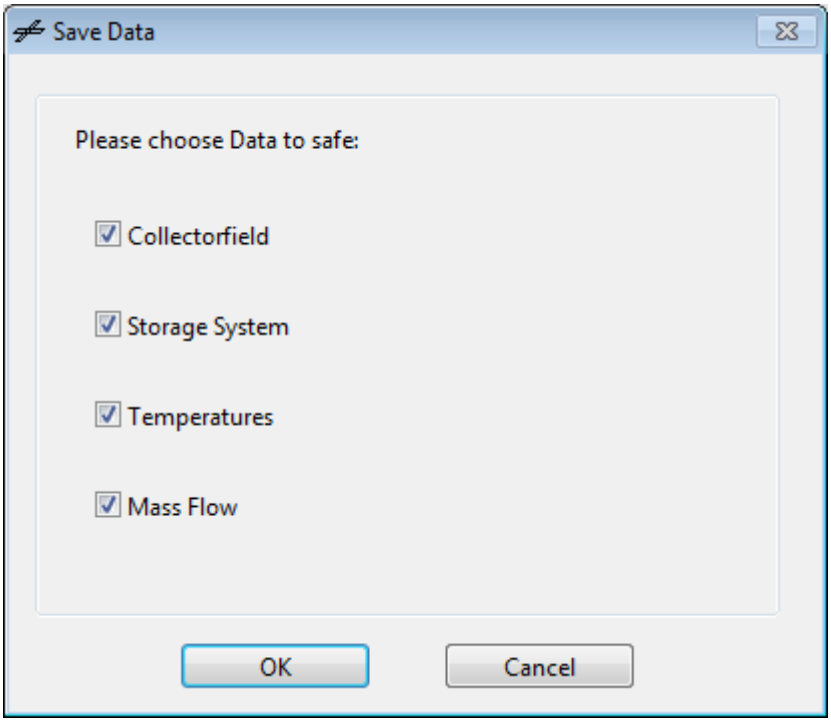

Figure 23: Save data window

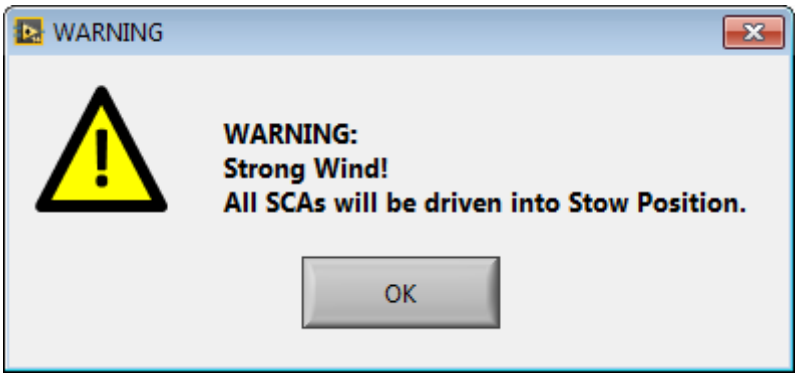

Figure 24: Exemplary pop-up warning